Two scale damage model and related numerical issues for thermo-mechanical high cycle fatigue

R. Desmorat[1], A. Kane[1], M. Seyedi [1*], J.P. Sermage[2]

[1] LMT-Cachan

61. avenue du Président Wilson

94235 Cachan - FRANCE

[2] EDF/R&D – LaMSID

1 avenue du Général de Gaulle

F-92141 Clamart Cedex, France

29 novembre 2006

Résumé

On the idea that fatigue damage is localized at the microscopic scale, a scale smaller than the mesoscopic one of the Representative Volume Element (RVE), a three-dimensional two scale damage model has been proposed for High Cycle Fatigue applications. It is extented here to anisothermal cases and then to thermo-mechanical fatigue. The modeling consists in the micromechanics analysis of a weak micro-inclusion subjected to plasticity and damage embedded in an elastic meso-element (the RVE of continuum mechanics). The consideration of plasticity coupled with damage equations at microscale, altogether with Eshelby-Kröner localization law, allows to compute the value of microscopic damage up to failure for any kind of loading, 1D or 3D, cyclic or random, isothermal or anisothermal, mechanical, thermal or thermo-mechanical. A robust numerical scheme is proposed in order to make the computations fast. A post-processor for damage and fatigue (DAMAGE_2005) has been developped. It applies to complex thermo-mechanical loadings. Examples of the representation by the two scale damage model of physical phenomena related to High Cycle Fatigue are given such as the mean stress effect, the non-linear accumulation of damage. Examples of thermal and thermo-mechanical fatigue as well as complex applications on real size testing structure subjected to thermo-mechanical fatigue are detailed.

1 Introduction

Various components of structures are subjected to thermo-mechanical loading during service. In nuclear power plants the operational feedback from PWRs has

*now at BRGM, Orléans, France

over the past few years pointed to some cases of cracking of austenitic stainless steel components attributed to thermal fatigue: safety injection system, between two check valves ; T-junction in the Residual Heat Removal System (RHRS) (Taheri and Doquet, 2001; Beaud et al., 2006; Faidy and Le-Duff, 2006; Robert et al., 2006). These events have led to increasing unavailability and to the setting up of costly programs to monitor, repair or replace the equipment affected. The situations encountered in the different structures are dependent on the time during which the T-junctions were operated with high temperature differences. Thermo-hydraulic and mechanical phenomena altogether explain qualitatively these thermal fatigue degradations (Curtit and Stephan, 2005; Taheri, 2007). The phenomena involved (thermal fatigue in imposed deformation, secondary hardening, high multiaxiality...) are nevertheless complex so that a quantitative analysis needs "sophisticated" prediction methods, for instance modeling heat exchange and variable amplitude multiaxial initiation conditions, with 3D metering method...

Models for computations of structures subjected to complex loadings, monotonic or not, are represented by constitutive equations often written in a rate form and in the thermodynamics framework (Lemaitre and Chaboche, 1985) when fatigue is usually addressed with specific engineering rules modeling directly the Wöhler curves of materials (Manson and Hirschberg, 1964; Aas-Jackobsen and Lenshow, 1973): a fatigue law can be a straight line in the log-log diagram of the maximum applied stress σ_{Max} vs the number of cycles to rupture N_R, curve generally parametrized by the stress ratio $R_\sigma = \sigma_{min}/\sigma_{Max}$ (with σ_{min} the minimum applied stress) or the mean stress $\overline{\sigma} = (\sigma_{min} + \sigma_{Max})/2$. In order to reproduce the effect of different mean stresses on Wöhler curves, amplitude laws function of the stress ratio are also often considered in fatigue damage models (Lemaitre and Plumtree, 1984; Hua and Socie, 1984; Chaboche and Lesne, 1988). The damage increment per cycle is set as a function of the current damage D, of the stress amplitude $\Delta\sigma = \sigma_{Max} - \sigma_{min}$ and of R_σ. The extension to 3D states of stresses of such modeling is not straightforward. What is then a stress amplitude? How to define a stress ratio? Neither is straightforward the extension to non cyclic loadings encountered in random fatigue or to thermo-mechnical complex loadings where the stresses and the temperature may vary independently. Last, the link between a stress and a strain formulation is not so clear for nonlinear materials, of course except if a rate written damage model is defined (Lemaitre and Chaboche, 1985; Paas, 1990; Lemaitre, 1992; Lemaitre and Desmorat, 2005) or if energetic considerations are taken into account (Dang-Van and Papadopoulos, 1999; Charkaluk and Constantinescu, 2000)

One proposes here to use the mean feature of Continuum Damage Mechanics in order to deal with complex loading in a quite simple (or at least natural) manner: damage and therefore the rupture process is considered as a full part of the material behavior. As it is the case for plasticity, it can be modeled by rate form written constitutive laws. The notion of cycles becomes then useless and such an approach avoids the need of more or less arbitrary rain-flow equivalent cycles count methods: peak count, mean crossing peak count, range count, range mean count, range pair count, level crossing count, rain-flow count...

Lemaitre damage law of a damage growth governed by plasticity and enhan-

ced by the elastic energy will used. A difficulty is to quantify plasticity in High Cycle Fatigue which is, at least at the Representative Volume Element (RVE) scale of continuum mechanics, a quasi non dissipative phenomenon. An efficient possibility of modeling has been proposed by Lemaitre and Doghri (1994): to consider that plasticity and damage occurs at the defects level, i.e. at a microscale smaller than the RVE-scale or mesoscale. A last difficulty is to propose robust and fast numerical schemes. Section 4 is devoted to this topic where an original scheme adapted to fatigue and random fatigue will be proposed. Compared to classical approaches for fatigue (Miner, 1945; Crossland, 1956; Dang-Van, 1973; Kujawski and Ellying, 1984; Manson and Halford, 1986; Leiholz, 1986; Leis, 1988; Zuchowski, 1989; Leis, 1997; Fatemi and Yang, 1998) the present Continuum Damage Mechanics approach allows for the quantification of damage, even in 3D, even for non cyclic thermo-mechanical loadings. It works as a post-processor of a reference thermo-elastic (or thermo-elasto-plastic) computation as detailed thereafter. It will be applied to complex structural thermo-mechanical fatigue cases: INTHERPOL mock up (Curtit, 2004; Curtit and Stephan, 2005) and FATHER real size experiments (these tests were performed by CEA, AREVA NP and EDF).

2 Two scale damage model

On the remark that High Cycle Fatigue, either thermally or mechanically activated, occurs for an elastic regime at the RVE scale, the mesoscale of continuum mechanics, a two scale damage model has been built (Lemaitre and Doghri, 1994; Lemaitre and Desmorat, 2001). It accounts for micro-plasticity and micro-damage at the defects scale or microscale. The model is phenomenological, describing micro-plasticity with classical 3D von Mises plasticity equations, describing micro-damage by Lemaitre damage evolution law $\dot{D} = (Y/S)^s \dot{p}$ of damage governed by the accumulated plastic strain rate $\dot{p}$, with Y the elastic energy density and S and s as damage parameters. A scale transition law makes the link between both mesoscopic and microscopic scales.

The general principles for building a two scale damage model for thermal and/or thermo-mechanical fatigue are as follows,

- at the mesoscale, the scale of the RVE of continuum mechanics, the behavior is considered as thermo-elastic, the material engineering yield stress σ_y being usually not reached in High Cycle Fatigue (accordingly called elastic fatigue),

- the microscale is the defects scale, defects conceptually gathered as a weak inclusion imbedded in previous RVE. The behavior at microscale is thermo-elasto-plasticity coupled with damage, the weakness of the inclusion being represented by a yield stress at microscale σ_y^μ taken equal to the asymptotic fatigue limit of the material σ_f^∞.

At the mesoscale, the stresses are denoted $\boldsymbol{\sigma}$, the total, elastic and plastic strains are $\boldsymbol{\epsilon}$, $\boldsymbol{\epsilon}^e$, $\boldsymbol{\epsilon}^p$. They are known from a thermo-elastic Finite Element (FE) computation as for High Cycle Fatigue $\boldsymbol{\epsilon}^p \approx 0$. The values at the microscale have an upper-script μ. For High Cycle Fatigue, with plasticity and damage assumed to

occur at the microscale only, one has $\boldsymbol{\epsilon}^{p\mu} \neq 0$, $0 \leq D < 1$, where for simplicity the damage variable at the microscale has no upper-script ($D = D^{\mu}$).

FIG. 1: *Micro-element imbedded in a thermo-elastic Representative Volume Element*

2.1 Thermo-elastic behavior at mesoscale

The thermoelastic law for the RVE reads

$$\boldsymbol{\epsilon} = \frac{1+\nu}{E}\boldsymbol{\sigma} - \frac{\nu}{E} tr\ \boldsymbol{\sigma}\ \mathbf{1} + \alpha(T - T_{ref})\mathbf{1} \tag{1}$$

with E the Young modulus, ν the Poisson ratio, α the thermal expansion coefficient and T_{ref} the reference temperature. The non homogeneous temperature and eventually time dependent field in a structure $T(\mathbf{x}, t)$ is usually determined from an initial heat transfer computation. The mechanical properties E, ν, α may depend on the temperature. The shear and bulk modulus of the material will respectively be $G = E/2(1+\nu)$ and $K = E/3(1-2\nu)$.

2.2 Plasticity and damage at microscale

A law of thermo-elasto-plasticity coupled with damage is considered at microscale. No viscosity is considered as for the applications in mind the temperature will remain much lower than one third of the melting temperature.

The elasticity law reads then (recall that μ-upper-script stands for "variable at microscale"):

$$\boldsymbol{\epsilon}^{\mu e} = \frac{1+\nu}{E}\frac{\boldsymbol{\sigma}^{\mu}}{1-D} - \frac{\nu}{E}\frac{tr\ \sigma^{\mu}}{1-D}\,\mathbf{1} + \alpha^{\mu}(T - T_{ref})\,\mathbf{1} \tag{2}$$

where the thermal expansion coefficient α^{μ} is taken next equal to the meso coefficient α. In the yield criterion, the hardening $\boldsymbol{X}^{\mu}$ is kinematic, linear, and the yield stress is the asymptotic fatigue limit of the material, denoted σ_f^{∞},

$$f^{\mu} = (\tilde{\boldsymbol{\sigma}}^{\mu} - \boldsymbol{X}^{\mu})_{eq} - \sigma_f^{\infty} \tag{3}$$

with $(.)_{eq}$ von Mises norm and where $\tilde{\boldsymbol{\sigma}}^{\mu} = \boldsymbol{\sigma}^{\mu}/(1-D)$ is the effective stress and where the elasticity domain is defined by $f^{\mu} < 0$. The set of constitutive equations at microscale is then:

$$\begin{cases} \boldsymbol{\epsilon}^{\mu} = \boldsymbol{\epsilon}^{\mu e} + \boldsymbol{\epsilon}^{\mu p} \\ \boldsymbol{\epsilon}^{\mu e} = \dfrac{1+\nu}{E}\tilde{\boldsymbol{\sigma}}^{\mu} - \dfrac{\nu}{E} tr\ \tilde{\boldsymbol{\sigma}}^{\mu}\mathbf{1} + \alpha(T - T_{ref})\,\mathbf{1} \\ \dot{\boldsymbol{\epsilon}}^{\mu p} = \dfrac{3}{2}\dfrac{\tilde{\boldsymbol{\sigma}}^{\mu D} - \boldsymbol{X}^{\mu}}{(\tilde{\boldsymbol{\sigma}}^{\mu} - \boldsymbol{X}^{\mu})_{eq}}\dot{p}^{\mu} \\ \dfrac{\mathrm{d}}{\mathrm{d}t}\left(\dfrac{\boldsymbol{X}^{\mu}}{C_y}\right) = \dfrac{2}{3}\dot{\boldsymbol{\epsilon}}^{\mu p}(1-D) \\ \dot{D} = \left(\dfrac{Y^{\mu}}{S}\right)^{s}\dot{p}^{\mu} \ \text{ if } \ p^{\mu} > p_D \\ D = D_c \longrightarrow \text{crack initiation} \end{cases} \tag{4}$$

with the plastic modulus C_y, the damage strength S, the damage exponent s as temperature dependent material parameters. A crack is initiated when D reaches the critical damage D_c. Note that in the isothermal case one hase $\dot{C}_y = 0$ and Prager linear kinematic hardening law is recovered as $\dot{\boldsymbol{X}}^\mu = \frac{2}{3} C_y (1-D) \dot{\boldsymbol{\epsilon}}^{\mu p}$.

The damage evolution is smaller in tension than in compression due to the consideration of the micro-defects closure parameter h within Y^μ as usually for metals $h \approx 0.2$ (Lemaitre, 1992; Lemaitre and Desmorat, 2005) and:

$$\begin{aligned} Y^\mu =& \frac{1+\nu}{2E} \left[\frac{\langle \boldsymbol{\sigma}^\mu \rangle^+ : \langle \boldsymbol{\sigma}^\mu \rangle^+}{(1-D)^2} + h \frac{\langle \boldsymbol{\sigma}^\mu \rangle^- : \langle \boldsymbol{\sigma}^\mu \rangle^-}{(1-hD)^2} \right] \\ & - \frac{\nu}{2E} \left[\frac{\langle tr\ \boldsymbol{\sigma}^\mu \rangle^2}{(1-D)^2} + h \frac{\langle -tr\ \boldsymbol{\sigma}^\mu \rangle^2}{(1-hD)^2} \right] \end{aligned} \tag{5}$$

$\langle \boldsymbol{\sigma}^\mu \rangle^+$ and $\langle \boldsymbol{\sigma}^\mu \rangle^-$ respectively denote the positive and negative parts of the stress tensor (in terms of principal values), $\langle x \rangle$ stands for the positive part of the scalar x, $\langle x \rangle = max(x, 0)$. In previous laws, p^μ is the accumulated plastic strain at micro-scale and p_D the damage threshold (for loading dependent threshold see next section or refer to (Lemaitre and Desmorat, 2005)). The plastic multiplier $\dot{\lambda} = \dot{p}^\mu (1-D)$ is determined from the consistency condition $f^\mu = 0$, $\dot{f}^\mu = 0$.

The internal variables $\boldsymbol{\epsilon}^{p\mu}$, p^μ, $D^\mu = D$ are usually considered equal to zero at $t = 0$. A pre-hardening or a pre-damage correspond to non vanishing initial values $\boldsymbol{\epsilon}^{p0}$, p_0, D_0 for the time integration of the differential equations (4).

2.3 Localization law coupled with damage and temperature

The scale transition meso $\rightarrow$ micro is governed by modified Eshelby-Kröner localization law (Eshelby, 1957; Kröner, 1961; Seyedi et al., 2004):

$$\begin{aligned} \boldsymbol{\epsilon}^{\mu D} &= \frac{1}{1-bD} \left[\boldsymbol{\epsilon}^D + b \left((1-D) \boldsymbol{\epsilon}^{\mu p} - \boldsymbol{\epsilon}^p \right) \right] \\ \epsilon_H^\mu &= \frac{1}{1-aD} \left[\epsilon_H + a \left((1-D) \alpha^\mu - \alpha \right) (T - T_{ref}) \right] \end{aligned} \tag{6}$$

$(.)^D = (.) - \frac{1}{3} tr\ (.)\ \mathbf{1}$ standing for the deviatoric part of a tensor, $(.)_H = \frac{1}{3} tr\ (.)$ for the hydrostatic part. By considering $\boldsymbol{\epsilon} = \boldsymbol{\epsilon}^D + \epsilon_H \mathbf{1}$, $\boldsymbol{\epsilon}^\mu = \boldsymbol{\epsilon}^{\mu D} + \epsilon_H^\mu \mathbf{1}$, the localization law reads:

$$\begin{aligned} \boldsymbol{\epsilon}^\mu =& \frac{1}{1-bD} \left[\boldsymbol{\epsilon} + \frac{(a-b)D}{3(1-aD)}\ tr\ \boldsymbol{\epsilon}\ \mathbf{1} + b \left((1-D) \boldsymbol{\epsilon}^{\mu p} - \boldsymbol{\epsilon}^p \right) \right] \\ & + \frac{a \left((1-D) \alpha^\mu - \alpha \right)}{1-aD} (T - T_{ref}) \mathbf{1} \end{aligned} \tag{7}$$

with a et b the Eshelby parameters for a spherical inclusion,

$$a = \frac{1+\nu}{3(1-\nu)}, \qquad b = \frac{2}{15} \frac{4-5\nu}{1-\nu} \tag{8}$$

Concerning these parameters, recall that if $\underline{\boldsymbol{S}}_E$ is Eshelby fourth order tensor, one has $\underline{\boldsymbol{S}}_E : \mathbf{1} = a\ \mathbf{1}$, $\underline{\boldsymbol{S}}_E : \boldsymbol{x}^D = b\ \boldsymbol{x}^D$, with $\mathbf{1}$ the unit tensor and $\boldsymbol{x}^D$ any deviatoric tensor.

2.4 Stored energy damage threshold

Damage in fatigue of metals usually does not initiate at the very begining of the loading so that one can distinguish 3 stages of degradation:

- a first stage of micro-plasticity and dislocations accumulation without (or with small) damage, i.e. $D \approx 0$,
- a second stage of micro-damage growth modeled by previous damage law, $\dot{D} \geq 0$,
- once damage reaches the critical value $D = D_c$ the meso-crack initiation and the third stage of crack propagation modeled with Fracture Mechanics tools.

One focus here on the first stage for which the accumulated plastic strain p_D^μ at damage initiation is loading dependent and cannot be considered as a material parameter. This feature is also characteristic of low cycle fatigue (Lemaitre and Desmorat, 2005) as the following general remark can be made for metals: in monotonic tension, the materials can undergo plasticity up to a plastic strain threshold $\epsilon_p = \epsilon_{pD}$ of the order of 10 to 30% when in fatigue it can take a few hundreds of percent of accumulated plastic strain before damage initiation (at $p = p_D$).

Such a loading dependency of the damage threshold can be represented by considering that damage initiates when the energy density stored by hardening w_s reaches the energetic damage threshold w_D, loading independent and considered as a material parameter, which is the amount of energy needed for the incubation of defects. According to plasticity framework, the stored energy density is defined as the integral (written here at microscale),

$$w_s^\mu = \int_0^t \left(\sigma_{eq}^\mu - \sigma_y^\mu\right) \dot{p}^\mu \, dt \tag{9}$$

with $\sigma_y^\mu = \sigma_f^\infty$ the fatigue limit. For monotonic loading, considering linear hardening $\sigma_{eq}^\mu \approx \sigma_y + C_y p^\mu$,

$$w_D = w_s^\mu(p = \epsilon_{pD}) = \left(\sigma_y - \sigma_f^\infty + \frac{1}{2} C_y \epsilon_{pD}\right) \epsilon_{pD} \approx \left(\sigma_u - \sigma_f^\infty\right) \epsilon_{pD} \tag{10}$$

with σ_u the ultimate stress and ϵ_{pD} the monotonic damage threshold in terms of plastic strain.

For fatigue, making the simplifying assumption $\sigma_{eq}^\mu \approx \sigma_{eq\,Max}^\mu$ (resp. $\sigma_{eq}^\mu \approx \sigma_{eq\,min}^\mu$) during the loading (resp. unloading) plastic part of the stress-strain cycle gives the damage threshold p_D^μ, loading dependent, as the solution of $w_s^\mu(p_D^\mu) = w_D$ with

$$w_s^\mu(p_D^\mu) = \int_0^{p_D^\mu} \left(\frac{\sigma_{eq\,Max}^\mu + \sigma_{eq\,min}^\mu}{2} - \sigma_f^\infty\right) dp^\mu = \left(\frac{(\Delta \boldsymbol{\sigma}^\mu)_{eq}}{2} - \sigma_f^\infty\right) p_D^\mu \tag{11}$$

or:

$$p_D^\mu = \epsilon_{pD} \cdot \frac{\sigma_u - \sigma_f^\infty}{\frac{(\Delta \boldsymbol{\sigma}^\mu)_{eq}}{2} - \sigma_f^\infty} \tag{12}$$

The time to crack initiation t_R is then the sum of two terms, the time to damage initiation $t_D = t(w_s^\mu = w_D)$ or for cyclic loadings $t_D = t(p^\mu = p_D^\mu)$ (first stage) and the time during which takes place the damage process (second stage).

3 Closed form expressions for isothermal fatigue

The previous set of differential equations can be integrated in a closed form for uniaxial fatigue (Desmorat and Lemaitre, 2001; Lemaitre and Desmorat, 2005). This can be done in two steps, 1) the time integration over one cycle to gain the plastic strain increment $\frac{\delta p^\mu}{\delta N}$ and the damage increment $\frac{\delta D}{\delta N}$ over this single cycle, 2) the integration with respect to the number of cycles N over the whole process. Two simplifying assumptions must be made: to consider the damage as constant over a cycle during the step 1) and to consider the stress triaxiality at microscale as constant equal to its maximum during a load or an unload. Note that maximum and minimum signed von Mises stresses do not vary much over a cycle as (Desmorat, 2000),

$$\begin{cases} \tilde{\sigma}^\mu_{Max} \approx \sigma_f^\infty + \dfrac{C_y(1-D)}{\mathcal{G}}(\sigma_{Max} - \sigma_f^\infty) \approx \sigma_f^\infty \\ \tilde{\sigma}^\mu_{min} \approx -\sigma_f^\infty + \dfrac{C_y(1-D)}{\mathcal{G}}(\sigma_{min} + \sigma_f^\infty) \approx -\sigma_f^\infty \end{cases} \tag{13}$$

where $\mathcal{G} = 3G(1-b) + C_y(1-D) \approx 3G(1-b)$. With $D = 0$ up to $N = N_D$, the number of cycles to damage initiation, given by previous stored energy based threshold ($p^\mu(N_D) = p_D$) in which $\frac{\Delta\sigma^\mu}{2} - \sigma_f^\infty = \frac{C_y}{\mathcal{G}}(\frac{\Delta\sigma}{2} - \sigma_f^\infty)$ is gained as a function of the stress amplitude $\Delta\sigma$ at mesoscale.

3.1 Calculation of Wöhler curve

For the isothermal uniaxial case, the number of cycles to rupture $N_R = N(D = D_c)$ is the number of cycles N_R for which $D = D_c$ is reached. For a stress varying cyclically between σ_{min} and σ_{Max},

$$\begin{aligned} N_R &= N_D + \frac{(2ES)^s \mathcal{G} D_c}{{\sigma_f^\infty}^{2s}\left[\Delta\sigma - 2\sigma_f^\infty\right]\left[R^s_{\nu min} + R^s_{\nu Max}\right]} \\ N_D &= \frac{1}{4}\epsilon_{pD}\frac{\mathcal{G}^2}{C_y}\frac{\left(\sigma_u - \sigma_f^\infty\right)}{\left(\dfrac{\Delta\sigma}{2} - \sigma_f^\infty\right)^2} \end{aligned} \tag{14}$$

with a stress amplitude $\Delta\sigma > 2\sigma_f^\infty$ for micro-plasticity to evolve and where one has set:

$$\begin{aligned} R_{\nu min} &= \frac{2}{3}(1+\nu) + \frac{1}{3}(1-2\nu)\left[\frac{\sigma_{min}}{\sigma_f^\infty}\right]^2 \\ R_{\nu Max} &= \frac{2}{3}(1+\nu) + \frac{1}{3}(1-2\nu)\left[\frac{\sigma_{Max}}{\sigma_f^\infty}\right]^2 \end{aligned} \tag{15}$$

The function $R_{\nu Max}$ (resp. $R_{\nu min}$) is the stress triaxiality function during loading at $\sigma = \sigma_{Max}$ (resp. at at $\sigma = \sigma_{min}$). In the closed form expression (14) the micro-defects closure parameter has been set equal to $h = 1$, i.e. no unilateral effect is taken into account. An even simpler formula is obtained for alternate fatigue with $\sigma_{min} = -\sigma_{Max}$ (zero mean stress $\overline{\sigma}$ or stress ratio $R_\sigma = \sigma_{min}/\sigma_{Max} = -1$) if the damage threshold is neglected ($p_D^\mu \approx 0$, $N_D \approx 0$),

$$N_R \approx \frac{(2ES)^s \mathcal{G} D_c}{4{\sigma_f^\infty}^{2s} \left[\sigma_{Max} - \sigma_f^\infty\right] R_{\nu Max}^s} \tag{16}$$

This last assumption of a vanishing damage threshold is often sufficient for practical applications (see for instances applications on INTHERPOL and FATHER structures, section 6). But anticipating section 3.3 results, it leads to linear Miner accumulation rule.

Note finally that the formula for shear fatigue can also be derived

$$\begin{aligned} N_R^{\text{shear}} &= N_D^{\text{shear}} + \left[\frac{3ES}{{\sigma_f^\infty}^2(1+\nu)}\right]^s \frac{\mathcal{G} D_c}{2(\sqrt{3}\Delta\tau - 2\sigma_f^\infty)} \\ N_D^{\text{shear}} &= \frac{1}{4}\epsilon_{pD}\frac{\mathcal{G}^2}{C_y}\frac{\left(\sigma_u - \sigma_f^\infty\right)}{\left(\dfrac{\sqrt{3}\Delta\tau}{2} - \sigma_f^\infty\right)^2} \end{aligned} \tag{17}$$

with $\Delta\tau$ the applied shear stress amplitude.

3.2 Mean stress effect and micro-defects closure parameter

The number of cycles to rupture in shear exhibits an important feature: as N_R^{shear} given by eq. (17) is function of the stress amplitude $\Delta\tau = \tau_{Max} - \tau_{min}$ and does not depend on the shear mean stress $\overline{\tau} = (\tau_{min} + \tau_{Max})/2$, no mean stress effect is recovered in shear fatigue, as observed from experiments (Sines, 1959; Shigley and Mischke, 1989).

For the tension-compression case and if the mean stress effect is of first importance it is better to use the two scale damage model with microcracks closure effect, i.e. to consider the micro-defects closure parameter $h < 1$ leading to a damage growth larger in tension than in compression. To gain again a closed form expression for the number of cycles to rupture, neglect the damage within the expression for the strain energy release rate (5), yielding:

$$Y^\mu \approx \frac{{\sigma_f^\infty}^2}{2E} R_{\nu h\star} \tag{18}$$

and also defining the triaxiality function $R_{\nu h\star}$ modified – compared to (15) – by the consideration of the microdefcts closure parameter h. In uniaxial ten-

sion/compression cases, one has:

$$R_{\nu h\star} = \frac{1+\nu}{9}\left[\left\langle 2+\frac{\sigma}{\sigma_f^\infty}\right\rangle^2 + 2\left\langle -1+\frac{\sigma}{\sigma_f^\infty}\right\rangle^2 + h\left\langle -2-\frac{\sigma}{\sigma_f^\infty}\right\rangle^2 + 2h\left\langle 1-\frac{\sigma}{\sigma_f^\infty}\right\rangle^2\right] - \nu\left\langle\frac{\sigma}{\sigma_f^\infty}\right\rangle^2 - \nu h\left\langle -\frac{\sigma}{\sigma_f^\infty}\right\rangle^2 \tag{19}$$

still with $\langle x\rangle$ the positive part of the scalar x.

The expression for N_R is formally the same as previously (Eq. 14) but with $R_{\nu\star}$ replaced by $R_{\nu h\star}$ for either $\sigma = \sigma_{Max}$ or $\sigma = \sigma_{min}$. The number of cycles $N_R(\overline{\sigma}, \Delta\sigma)$ for a given mean stress and a given stress amplitude can be compared to the number of cycles $N_R(\overline{\sigma} = 0, \Delta\sigma)$ for a zero mean stress but for the same stress amplitude $\Delta\sigma = \sigma_{Max} - \sigma_{min} = 2\sigma^0_{Max}$ calculated either for a mean stress using σ_{Max}, σ_{min} or from a zero mean stress using $\sigma^0_{Max} = -\sigma^0_{min}$,

$$\frac{N_R(\overline{\sigma}, \Delta\sigma)}{N_R(\overline{\sigma} = 0, \Delta\sigma)} = \frac{R^s_{\nu h\star}(\sigma^0_{Max}) + R^s_{\nu h\star}(\sigma^0_{min})}{R^s_{\nu h\star}(\sigma_{Max}) + R^s_{\nu h\star}(\sigma_{min})} \tag{20}$$

in which the damage threshold has been neglected. The curve $N_R(\overline{\sigma}, \Delta\sigma)/N_R(\overline{\sigma} = 0, \Delta\sigma)$ versus the stress amplitude normalized by twice the asymptotic fatigue limit $\Delta\sigma/\sigma_f^\infty$ is given in Fig. 2 for different mean stress normalized by the fatigue limit ratios $\overline{\sigma}/\sigma_f^\infty$. The horizontal constant line $N_R(\overline{\sigma}, \Delta\sigma)/N_R(\overline{\sigma} = 0, \Delta\sigma) = 1$ corresponds to no mean stress effect. A reduction in fatigue life due to positive mean stresses is obtained ($N_R(\overline{\sigma} > 0, \Delta\sigma)/N_R(\overline{\sigma} = 0, \Delta\sigma) < 1$, solid lines). Similarly, an increase of the fatigue life due to negative mean stresses is obtained ($N_R(\overline{\sigma} < 0, \Delta\sigma)/N_R(\overline{\sigma} = 0, \Delta\sigma) > 1$, dash lines). Two values $s = 1$ and $s = 2$ of the damage exponent are considered exhibiting the sensitivity to this parameter, a higher s amplifies the mean stress effect.

To conclude, one has shown by the present analysis that the two scale damage model qualitatively represents the mean stress effect in tension/compression when the micro-defects closure parameter h is considered.

FIG. 2: *Mean stress effect – Curves plotted at constant ratio $\overline{\sigma}/\sigma_f^\infty$ for two values of the damage exponent s*

3.3 Nonlinear damage accumulation

The accumulation of damages due to two successive loadings with different stress ranges $\Delta\sigma_1$ and $\Delta\sigma_2$ is simply obtained from the remark that the previous closed form expressions correspond to a damage increment per cycle $\frac{\delta D}{\delta N}$ constant for a given stress amplitude and a given mean stress. Therefore, one has for each single level loading (denoted i, $i = 1$ or 2),

$$\frac{\delta D}{\delta N} = \frac{D_c}{N_{Ri} - N_{Di}} \tag{21}$$

For a two level fatigue loading made of n_1 cycles at $\Delta\sigma = \Delta\sigma_1$ and $\overline{\sigma} = \overline{\sigma}_1$ followed by n_2 cycles at $\Delta\sigma = \Delta\sigma_2$ and $\overline{\sigma} = \overline{\sigma}_2$, two cases occur for the damage accumulation:

1. the damage initiates at $N = N_{D1}$ cycles (gained from the stored energy threshold) during the first loading,
2. the damage initiates at $N = N_D$ cycles (still gained from the stored energy threshold and different from N_{D1} and N_{D2}).

In the first case, the number of cycles to rupture for the two level loading, $N_R = n_1 + n_2$, is the solution of the damage accumulation up to $D = D_c$.

$$\frac{D_c}{N_{R1} - N_{D1}}(n_1 - N_{D1}) + \frac{D_c}{N_{R2} - N_{D2}} n_2 = D_c \tag{22}$$

In the second case, N_R is the solution of

$$\frac{D_c}{N_{R1} - N_{D1}} n_1 + \frac{D_c}{N_{R2} - N_{D2}}(n_2 - N_D) = D_c \tag{23}$$

with N_D determined from the continuity of both expression at $n_1 = N_{D1}$. A bilinear damage accumulation is finally obtained for a non zero damage threshold as

$$\begin{aligned} &\frac{n_1}{N_{R1}} + \frac{n_2}{N_{R2}} \frac{1 - \dfrac{N_{D1}}{N_{R1}}}{1 - \dfrac{N_{D2}}{N_{R2}}} = 1 \qquad \text{if} \quad n_1 \leq N_{D1} \\ &\frac{n_1}{N_{R1}} \frac{N_{D2}}{N_{D1}} \frac{N_{R1}}{N_{R2}} + \frac{n_2}{N_{R2}} = 1 \qquad \text{if} \quad n_1 > N_{D1} \end{aligned} \tag{24}$$

Note that the linear Miner rule is recovered if there is no damage threshold ($w_D = 0$) or more generally if the ratio N_D/N_R of the number of cycles to damage initiation divided by the number of cycles to rupture has a loading independent constant value.

4 Numerical scheme for anisothermal two scale damage model

Structures subjected to High Cycle Fatigue are most often structures loaded in the elastic or thermo-elastic domain (at the RVE scale). The strains, the stresses and the temperature at mesoscale can then be determined from a (thermo-)elastic Finite Element computation. They are the inputs of the post-processor DAMAGE_2005 which performs the time integration of the constitutive equations of the two scale damage model up to the reach of the critical damage $D = D_c$ (crack initiation condition). The originality of the present post-processor is that it can handle the thermal effects. A new implicit scheme is proposed – still for efficiency reasons – and described next, the idea being to avoid the use of Newton scheme when solving plasticity coupled with damage equations.

The strain and temperature histories at mesoscale are then known from a reference Finite Element thermoelastic computation. The numerical scheme is classically strain driven: at each time step t_{n+1} and for known strain increment at mesoscale $\Delta\boldsymbol{\epsilon} = \boldsymbol{\epsilon}_{n+1} - \boldsymbol{\epsilon}_n$ and temperature increment $\Delta T = T_{n+1} - T_n$, the numerical scheme must calculate, by time integration of the constitutive equations at microscale altogether with the consideration of the localization law, the strain $\boldsymbol{\epsilon}^{\mu}_{n+1}$, stress $\boldsymbol{\sigma}^{\mu}_{n+1}$, plastic strain $\boldsymbol{\epsilon}^{\mu p}_{n+1}$, accumulated plastic strain p^{μ}_{n+1} and damage D_{n+1} at microscale.

4.1 Euler Backward scheme explicited for the two scale damage model

The 3 stages for the numerical resolutions of the model equations classically are: 1) an elastic prediction at microscale, taking into account the localization law, 2) a test over the criterion function f^{μ}, and 3) if the criterion f^{μ} is found positive, a plastic-damage correction (still at microscale). For the last stage, Euler backward scheme will be used with the advantage in case of non anisothermal loading to already know the temperature at time t_{n+1}, therefore to know the value of the material parameters.

4.1.1 Elastic Prediction

The elastic prediction assumes a behavior (thermo-)elastic with constant plastic strain $\boldsymbol{\epsilon}^{\mu p}_{n+1} = \boldsymbol{\epsilon}^{\mu p}_{n}$, constant kinematic hardening $\boldsymbol{X}^{\mu}_{n+1} = \boldsymbol{X}^{\mu}_{n}$ and constant damage $D_{n+1} = D_n$. The elastic prediction gives a first estimate for the total strain, the elastic strain and the effective stress at microscale at time t_{n+1},

$$
\begin{aligned}
\boldsymbol{\epsilon}^{\mu} =& \frac{1}{1-bD_n}[\boldsymbol{\epsilon}_{n+1} + \frac{(a-b)D_n}{3(1-aD_n)}\, tr\, \boldsymbol{\epsilon}_{n+1}\, \mathbf{1} \\
&+ b\left((1-D_n)\boldsymbol{\epsilon}^{\mu p}_{n} - \boldsymbol{\epsilon}^{p}_{n+1}\right)] \\
&+ \frac{a\left((1-D_n)\alpha^{\mu}_{n+1} - \alpha_{n+1}\right)}{1-aD_n}(T_{n+1} - T_{ref})\mathbf{1} \\
\boldsymbol{\epsilon}^{\mu e} =& \boldsymbol{\epsilon}^{\mu} - \boldsymbol{\epsilon}^{\mu p}_{n} - \alpha^{\mu}_{n+1}(T_{n+1} - T_{ref})\mathbf{1} \\
\tilde{\boldsymbol{\sigma}}^{\mu} =& \underline{\underline{\boldsymbol{E}}} : \boldsymbol{\epsilon}^{\mu e} \\
\boldsymbol{\sigma}^{\mu} =& (1-D_n)\tilde{\boldsymbol{\sigma}}^{\mu}
\end{aligned}
\tag{25}
$$

where $\underline{\underline{\boldsymbol{E}}}_{n+1} = \underline{\underline{\boldsymbol{E}}}(T_{n+1})$ is Hooke's tensor and $\alpha_{n+1} = \alpha(T_{n+1})$ is the thermal expansion coefficient at temperature T_{n+1} at time t_{n+1}.

4.1.2 Plastic-damage correction

The previous elastic prediction gives the estimate $\tilde{\boldsymbol{\sigma}}$ of the effective stress $\tilde{\boldsymbol{\sigma}}_{n+1}$ at time t_{n+1}, with unchanged kinematic hardening $\boldsymbol{X} = \boldsymbol{X}_n$, and allows for the calculation of the yield criterion. If the condition $f^{\mu}_{n+1} \leq 0$ is fulfilled, the calculation is over and $\boldsymbol{\epsilon}^{\mu p}_{n+1} = \boldsymbol{\epsilon}^{\mu p}_{n}$, $\boldsymbol{X}_{n+1} = \boldsymbol{X}_n$, $D_{n+1} = D_n$ is set. If not, this elastic solution is corrected by ensuring the consistency condition $f^{\mu}_{n+1} = 0$ (resolution by Euler implicit scheme).

For non monotonic application, it is judicious to assume damage constant over a time increment. In High Cycle Fatigue, D could even be considered as constant over a full cycle (Lemaitre, 1992) as if N_R cycles are necessary to break the material, the maximum damage increment per cycle is of the order of magnitude of $D_c/N_R < 1/N_R$, small value indeed!

The set of plasticity coupled with damage equations (4) discretized by use of Euler backward scheme is now:

$$\begin{cases} \boldsymbol{\epsilon}^{\mu}_{n+1} = \boldsymbol{\epsilon}^{\mu e}_{n+1} + \boldsymbol{\epsilon}^{\mu p}_{n+1} \\ \boldsymbol{\epsilon}^{\mu e}_{n+1} = \dfrac{1+\nu}{E_{n+1}} \tilde{\boldsymbol{\sigma}}^{\mu}_{n+1} - \dfrac{\nu}{E_{n+1}} tr\ \tilde{\boldsymbol{\sigma}}^{\mu}_{n+1} \mathbf{1} + \alpha^{\mu}_{n+1}(T_{n+1} - T_{ref})\ \mathbf{1} \\ \Delta\boldsymbol{\epsilon}^{\mu p} = \dfrac{3}{2} \dfrac{\tilde{\boldsymbol{\sigma}}^{\mu D}_{n+1} - \boldsymbol{X}^{\mu}_{n+1}}{(\tilde{\boldsymbol{\sigma}}^{\mu}_{n+1} - \boldsymbol{X}^{\mu}_{n+1})_{eq}} \Delta p^{\mu} \\ \dfrac{\boldsymbol{X}^{\mu}_{n+1}}{C_{n+1}} - \dfrac{\boldsymbol{X}^{\mu}_{n}}{C_n} = \dfrac{2}{3} \Delta\boldsymbol{\epsilon}^{\mu p}(1 - D_n) \\ \Delta D = \left(\dfrac{Y^{\mu}_{n+1}}{S_{n+1}} \right)^{s_{n+1}} \Delta p^{\mu} \end{cases} \tag{26}$$

with $E_{n+1} = E(T_{n+1})$, $S_{n+1} = S(T_{n+1})$, $s_{n+1} = s(T_{n+1})$, $C_{n+1} = C_y(T_{n+1})$ the material parameters at time t_{n+1} (and $C_n = C_y(T_n)$) so that the discretized set of constitutive equations coupled with the scale transition law can be rewritten

$$\begin{aligned} &\Delta\boldsymbol{\epsilon}^{\mu e} + \frac{1-b}{1-bD_n} \Delta\boldsymbol{\epsilon}^{\mu e} + \alpha^{\mu}_{n+1} \Delta T \mathbf{1} - \frac{1}{1-bD_n} \Delta\boldsymbol{\epsilon} + \frac{b}{1-bD_n} \Delta\epsilon^{p} \\ &- \frac{(a-b)D_n}{(1-bD_n)(1-aD_n)} tr\ \Delta\epsilon \mathbf{1} - \frac{a\left((1-D_n)\alpha^{\mu}_{n+1} - \alpha_{n+1}\right)}{1-aD_n} \Delta T \mathbf{1} = 0 \\ &f^{\mu}_{n+1} = (\tilde{\boldsymbol{\sigma}}^{\mu}_{n+1} - \boldsymbol{X}^{\mu}_{n+1})_{eq} - \sigma^{\infty}_{f} = 0 \end{aligned} \tag{27}$$

These equations can of course be solved by use of Newton iterative method, but to write them in the form of 2 residuals R_p and $\boldsymbol{R}_s$ function of the unknown accumulated plastic strain and of the unknown variable $\boldsymbol{s}^{\mu} = \tilde{\boldsymbol{\sigma}}^{\mu}_{n+1} - \boldsymbol{X}^{\mu}_{n+1}$ allows to explicitly gain a closed-form solution,

$$\begin{cases} \boldsymbol{R}_s &= \dfrac{\boldsymbol{s}^{\mu}_{n+1}}{E_{n+1}} + \Gamma' \dfrac{\boldsymbol{s}^{\mu D}_{n+1}}{(\boldsymbol{s}^{\mu}_{n+1})_{eq}} \Delta p^{\mu} + \boldsymbol{Q}_s = 0 \\ R_p &= (\boldsymbol{s}^{\mu}_{n+1})_{eq} - \sigma^{\infty}_{f} = 0 \end{cases} \tag{28}$$

One has set in previous equations:

$$\begin{aligned} \boldsymbol{Q}_s =& \frac{C_{n+1}\boldsymbol{X}^{\mu}_{n}}{C_n E_{n+1}} - \frac{\tilde{\boldsymbol{\sigma}}^{\mu}_{n}}{E_{n+1}} \\ &- \frac{1}{1-bD_n} \left[\underline{\boldsymbol{E}}' : \Delta\boldsymbol{\epsilon} + K' \frac{(a-b)D_n}{1-aD_n} tr\ \Delta\boldsymbol{\epsilon}\mathbf{1} - 2G'b\Delta\boldsymbol{\epsilon}^{p} \right] \\ &+ \frac{3K'}{(1-aD_n)} \left((1-a)\alpha^{\mu}_{n+1} + a\alpha_{n+1} \right) \Delta T \mathbf{1} \\ \Gamma' =& \frac{1}{E_{n+1}} \left(3G_{n+1} \frac{1-b}{1-bD_n} + C_{n+1}(1-D_n) \right) \end{aligned} \tag{29}$$

with the notations $\underline{\underline{\boldsymbol{E}}}' = \underline{\underline{\boldsymbol{E}}}(T_{n+1})/E_{n+1}$, $G' = G(T_{n+1})/E_{n+1}$, $K' = K(T_{n+1})/E_{n+1}$ not standing for derivatives but for nomalized quantities (the normalization with respect to the Young modulus altogether with the consideration of a constant Poisson ratio make those tensors temperature independent). The quantities G and K are respectively the shear modulus and the compressibility modulus of the material.

The exact solution of (27) rewritten as (28) is:

$$\begin{aligned} s^{\mu}_{H\ n+1} &= -E_{n+1}Q_{sH} \\ \Delta p^{\mu} &= \frac{1}{\Gamma'}\left(Q_{seq} - \frac{\sigma_f^{\infty}}{E_{n+1}}\right) \\ \boldsymbol{s}^{\mu D}_{n+1} &= -\frac{E_{n+1}\boldsymbol{Q}_s^D}{1 + \dfrac{\Gamma' E_{n+1}}{\sigma_f^{\infty}}\Delta p^{\mu}} \end{aligned} \tag{30}$$

with the exponent ^{D} for the deviatoric part, Q_{seq} for von Mises norm of tensor $\boldsymbol{Q}_s$,Q_{sH} for its hydrostatic part and with $\boldsymbol{s}^{\mu}_{n+1} = \boldsymbol{s}^{\mu D}_{n+1} + s^{\mu}_{H\ n+1}\,\mathbf{1}$.

4.1.3 Variables updating

Once the previous correction made, all the variables at microscale are updated as follows,

- normal to the yield surface: $\boldsymbol{m}^{\mu} = \dfrac{3}{2}\dfrac{\boldsymbol{s}^{\mu D}_{n+1}}{\sigma_f^{\infty}}$
- plastic strain : $\boldsymbol{\epsilon}^{\mu p}_{n+1} = \boldsymbol{\epsilon}^{\mu p}_{n} + \boldsymbol{m}^{\mu}\Delta p^{\mu}$
- kinematic hardening:
  $\boldsymbol{X}^{\mu}_{n+1} = \dfrac{2}{3}C_{n+1}(1-D_n)\Delta\boldsymbol{\epsilon}^{\mu p}_{n+1} + \dfrac{C_{n+1}}{C_n}\boldsymbol{X}^{\mu}_{n}$
- effective stress: $\tilde{\boldsymbol{\sigma}}^{\mu}_{n+1} = \boldsymbol{s}^{\mu}_{n+1} + \boldsymbol{X}^{\mu}_{n+1}$
- elastic strain: $\boldsymbol{\epsilon}^{\mu e}_{n+1} = \underline{\underline{\boldsymbol{E}}}^{-1} : \tilde{\boldsymbol{\sigma}}^{\mu}_{n+1} + \alpha^{\mu}_{n+1}(T_{n+1} - T_{ref})\mathbf{1}$
- damage:
  $D_{n+1} = D_n + \left(\dfrac{Y^{\mu}_{n+1}}{S_{n+1}}\right)^{s_{n+1}}\Delta p^{\mu}$ if $p > p_D$ with

$$\begin{aligned} Y^{\mu}_{n+1} =& \frac{1+\nu}{2E_{n+1}}[\langle\tilde{\boldsymbol{\sigma}}^{\mu}_{n+1}\rangle^{+} : \langle\tilde{\boldsymbol{\sigma}}^{\mu}_{n+1}\rangle^{+} + h\left(\frac{1-D_n}{1-hD_n}\right)^2\langle\tilde{\boldsymbol{\sigma}}^{\mu}_{n+1}\rangle^{-} : \langle\tilde{\boldsymbol{\sigma}}^{\mu}_{n+1}\rangle^{-}] \\ & - \frac{\nu}{2E_{n+1}}[\langle tr\ \tilde{\boldsymbol{\sigma}}^{\mu}_{n+1}\rangle^2 + h\left(\frac{1-D_n}{1-hD_n}\right)^2\langle -tr\ \tilde{\boldsymbol{\sigma}}^{\mu}_{n+1}\rangle^2] \end{aligned} \tag{31}$$

- stress tensor : $\boldsymbol{\sigma}^{\mu}_{n+1} = (1-D_{n+1})\tilde{\boldsymbol{\sigma}}^{\mu}_{n+1}$

and one can then start the calculation at time t_{n+2}.

As mentioned earlier and as a important feature for fatigue, Euler Backward scheme is used but due to the above calculations the discretized equations are solved with no need of an iterative process. Recall to conclude that the scheme has been detailed on one time step and that it applies to complex loading, complex meaning for instance multiaxial, non proportional, anisothermal...

4.2 DAMAGE_2005 post-processor

A Fortran program solves the two scale model constitutive equations with previous numerical scheme. For a given material parameters file and for a given loading sequence, the program calculates the time to crack initiation, i.e. the time to reach the critical damage D_c. The inputs (mesostrains and temperature) come from a Finite Element reference computation and are then exported at user chosen Gauss points. The maximum number of instants used to describe a cycle being large (actually 5000), the program allows for quasi-random fatigue calculations.

The first release of the two scale damage and fatigue post-processor was LMT-Cachan DAMAGE_90 program (Lemaitre and Doghri, 1994), followed by DAMAGE_98 (Lemaitre et al., 1999), DAMAGE_2000 (Sauzay, 2000). The mean feature of fatigue such as the mean stress effect, the non-linear accumulation of damage, initial hardening effect and the non proportional loading effect in bi-axial fatigue were recovered. Only the new DAMAGE_2005 release allows for anisothermal conditions, as illustrated in next application sections. A graphical interface and a semi-automatic identification procedure (coupling Fortran, Python and Glade files) has been programmed for efficient applications, for instance for assisted identification and results plotting (Desmorat et al., 2006). The outputs of any calculation are a standard results file (damage history), and optional files for complete results at mesoscale and microscale.

4.3 Material parameters identification

For the material parameters identification, the following procedure may be used.

1. The mesoscale parameters (E, ν, α, σ_y, C_y) are identified at each temperature on the monotonic tensile curves.

2. The asymptotic fatigue limit is guessed from an experimental Wöhler curve as the "asymptote" at very high numbers of cycles. Note that for a non symmetric fatigue loading with a stress ratio $R_\sigma = \sigma_{min}/\sigma_{Max} \neq -1$, the asymptote $\sigma_{Max} = \sigma^\infty_{Max}$ obtained by the model corresponds to $\Delta\sigma = 2\sigma^\infty_f$ and gives the – material parameter – fatigue limit σ^∞_f as:

$$\sigma^\infty_f = \frac{1}{2}(1 - R_\sigma)\sigma^\infty_{Max} \tag{32}$$

3. Take for the parameters h and D_c the default constant values for metals, $h = 0.2$, $D_c = 0.3$ (Lemaitre, 1992).

4. The damage parameters S and s are pre-identified from a nonlinear fitting (Fig. 3): the experimental Wöhler curve entered as a text file (reference curve) and the approximate closed-form solution (14) for the number of cycles to rupture is used to obtain automatically a first set of parameters S, s .

5. The value for s is kept when the parameter S is adjusted by comparison with the reference curve but using this time DAMAGE_2005 to compute the Wöhler curve instead of the approximate formula (Fig. 4).

FIG. 3: *Fast identification procedure from approximate formula (14) with* $h = 1$

FIG. 4: *Final identification of* S *with* $h = 0.2$

Once the material parameters identified as well as their temperature dependency, the computations of structures subjected to complex loadings are performed by saving on user's demand the results at mesoscale and/or at microscale for later curves plotting (microstresses or damage history over a complex cycle for instance, see next examples on FATHER and INTHERPOL applications).

5 Thermal and thermo-mechanical fatigue

5.1 Thermal fatigue

A first simple academic case to illustrate the anisothermal facilities of the model and the corresponding post-processor is the example of a bar blocked at its two extremities and uniformly heated and cooled (Fig. 5). The corresponding thermal fatigue loading is assumed homogeneous, it is:

$$T = T(t), \quad \epsilon_1 = 0, \quad \epsilon_2 = \epsilon_3 = \alpha(1+\nu)(T - T_{ref}) \tag{33}$$

where the temperature varies between a minimum value T_{min} and a maximum value T_{Max} and with $T_{ref} = (T_{Max} - T_{min})/2 = 150°\text{C}$. Micro-plasticity (and damage) occurs from points A to B, C to D, E to next summit, with elastic stages at microscale in-between. The numbers of cycles to rupture $N_R = N(D = D_c)$ are plotted in Fig. 6 thanks to DAMAGE_2005 post-processor, the input loading being Eq. (33). This is the computed thermal fatigue curve T_{Max} vs N_R (with here $T_{min} = T_{ref} = 150°\text{C}$).

FIG. 5: *Thermal fatigue of a beam*

FIG. 6: *Computed thermal fatigue curve*

5.2 An example of thermo-mechanical fatigue

Complex thermo-mechanical loadings are encountered in real structures. As an illustration, one proposes here to calculate the time to rupture of a pipe subjected to both temperature $T(t)$ and internal pressure $P(t)$ variations. The cylinder is assumed thin, the temperature uniform. The stresses due to the thermal loading and to the mechanical loading are of the same order of magnitude. The cyclic applied temperature is assumed linear (linear increasing stage followed by a linear decrease) at a frequency f_0 between a minimum temperature T_{min} and a maximum temperature T_{Max}. Using the periodic piecewise linear triangle function triangle(x) (triangle(0) = triangle(1) = 0, triangle($\frac{1}{2}$) = 1, period 1s)

$$T(t) = T_{min} + \Delta T \cdot \text{triangle}(f_0 t) \tag{34}$$

where $\Delta T = T_{Max} - T_{min}$ is the applied temperature amplitude.

FIG. 7: *Thermomechanical fatigue of a pipe with internal pressure*

Different pressure loadings are considered :

- constant : $P = P_{Max}$,
- in phase with the temperature (case 1): $P = 0$ for $T = T_{min}$, $P = P_{Max}$ for $T = T_{Max}$ or
$$P(t) = P_{Max} \cdot \text{triangle}(f_0 t) \tag{35}$$
- out of phase with the temperature (case 2) : $P = 0$ for $T = T_{Max}$, $P = P_{Max}$ for $T = T_{min}$ or
$$P(t) = P_{Max} \cdot \text{triangle}\left(f_0 t - \frac{f_0}{2}\right) \tag{36}$$

The results – independent from the frequency due to the plasticity modeling – are given in Fig. 8 still assuming homogeneous strain and temperature fields for the different pressure variations (either constant at $P = P_{Max}$ or varying in phase or out of phase with the temperature). Recall that ΔT is the applied temperature amplitude and one has set for the computations the maximum pressure $P_{Max} = 5$ MPa and the mean temperature $\overline{T} = T_{ref} = (T_{Max} + T_{min})/2 = 150°\text{C}$. A strong effect of temperature-pressure out of phase loading on the number of cycles to rupture is obtained, comforting us in the idea that one must develop adequate tools for anisothermal thermo-mechanical cases.

FIG. 8: *Thermomechanical fatigue – in phase (case 1), out of phase (case 2) loadings and loadings at constant pressure*

6 Anisothermal structures computations

Turbulent mixing of hot (up to 170°C) and cold (room temperature) water in stainless steel pipes of nuclear power plants may generate networks of thermal fatigue cracks on the inner surface of some pipes . The temperature fields in the pipes are quite complex varying almost randomly as are the almost random stresses generated by the turbulent mixing (Taheri, 2004; Curtit, 2004; Angles et al., 2005). In order to evaluate the risk of crack initiation and crack development and due to the complexity of the problem, the realization of several fatigue tests with thermal loadings has been developed in the framework of a European project "THERFAT" gathering industrials (EDF, CEA and AREVA NP) and research centers around the problems of thermal fatigue of mixing zones. The complexity of such in-service experiences is illustrated in Figure 9 where a turbulent mixing zone occurs and where the thermal fatigue cracks seems to occur arbitrarily in any pipes branch at the T-connection.

FIG. 9: *Turbulent temperature mixing in T-configuration*

6.1 Application to FATHER experiment

An experimental structure test called "FATHER", representative of the geometry, the material and the loading in some piping system Tee-connections has been developed (figures 9 and 10)). In such a test, the hot fluid mass flow in the horizontal branch do not instantaneously mix with the cold fluid mass flow at the intersection with the vertical run pipe. Hot streak oscillates in the cold mass flow causing fatigue for significant hot/cold temperature differences in the adjacent pipe components. The material of the pipe is the AISI 304L steel. The strains (and the stresses) in the pipe are due to the thermal fluctuations, random around an average temperature, non uniaxial and with an observed non-zero mean strain. The complete loading is due to both internal pressure and thermal stresses; it varies in a large scale along the pipe.

The stresses determination in the T-connection derives from a Finite Element modeling of the turbulent temperature mixing effects (Pasutto et al., 2005) Temperatures measurements in the inner surface of the wall allowed to properly model the thermal exchanges due to heat flux in the wall. It allowed for the correct evaluation of the strains on the inner surface.

From the experiment, we have at our disposal temperature measurements at points on the outer surface of the solid wall as well as measurements due to thermocouples of the brazen combined corks on the inner surface. But note that due to the high radial temperature gradients across the walls thickness, the comparison between thermo-elastic computations and experiments must be stated with care and further validation works are in progress. They will next be considered as the known inputs for DAMAGE_2005 post-processor as they give the temperature and the strain histories at different points of FATHER structure, therefore at the RVE mesoscale of the two scale damage analysis.

FIG. 10: *FATHER testing structure and computed instantaneous non dimensional temperature field(time=10s)*

A limited number of points of interest are defined. An adequate designation is adopted to mark them, as follows,

- the angles origin is the inferior generatrix,
- the angles are counted positively in trigonometric sense tracing the downstream section of the flow. North angles are positive and conversly South angles are negative.
- the points position is designed as C (annulus number) (angle value)_(i_ for internal or _e for external). The angle value is expressed using the form of "a character followed by the absolute value of an angle". The characters are either "m" for negative angles or "p" for positive angles.

To clarify the notation and as an example, C11_m60i is the designation of an interest point located in the internal surface on the annulus C11 at the angle value of -60°. There is no difference, as for the positions of measures, between North and South positions (or to the left and to the right according to the flow) for a simple reason that in terms of computation a symmetry all around vertical plane has been assumed.

The FATHER structure has been examined by inspections during testing. The information available are detections of cracks by ultrasounds from the outer surface. For each measurement point and due to computational cost, the history of the strains and of the corresponding temperatures is obtained over a duration of a maximum of 10 seconds using Finite Element analyses. Aiming at predicting the risks and times of appearance of the first crack and as already pointed out, these (thermo-elastic) numerical results are then the inputs of the two scale damage model through the use of DAMAGE_2005 post-processor. These Finite Element results gained over 10 seconds of loading are transformed into a quasi-random cycle made of the temperature and strains history defined step by step by 1000 instants (Fig. 11). The cycle is then repeated into DAMAGE_2005 up to the reach of the critical damage D_c at one point.

FIG. 11: *Loading sequence made of 1000 instants*

Austenitic steel 304L used for the FATHER experiment has been subjected to numerous fatigue tests in aerial as well as aqueous (REP) media (Dupas and Waeckel, 1997), whose data allowed for the identification of the material (damage) parameters for the two scale model. The parameters were especially determined at 20, 150 et 300°C from the experimental Wöhler curves set up for the condition of polished surface in aqueous medium. The corresponding material parameters are given in tables 1 and 2. The reference parameter is $T_{ref} = 20°C$.

The damage post-processing is then made by assuming a linear interpolation of the material parameters between these temperatures through the use of

TAB. 1: *Temperature independent parameters for 304L steel*

ν	D_c	ϵ_{pD}	h
0.3	0.3	0	0.2

TAB. 2: *Temperature dependent parameters for 304L steel*

T (°C)	E (MPa)	C_y (MPa)	α (/°C)	S (MPa)	s	σ_f^∞ (MPa)
20	197000	1740	$1.65\ 10^{-5}$	3	2	180
150	188000	1824	$1.76\ 10^{-5}$	2	2	170
300	176000	1910	$1.88\ 10^{-5}$	2	2	169

DAMAGE_2005. The final results are thereafter compared to the experimental observations as the computed times to crack initiation at the differents points normalized by the observed time to crack initiation $t^{\text{exp}}_{\text{C11m80i}}$ close to point C11_m80i. The relative times to crack initiation obtained from the repeated 10 seconds sequence are given in table 3 for the different points of interest. The two values considered for the time $t^{\text{exp}}_{\text{C11m80i}}$ corresponds to the times of the successive inspections n and $n+1$ between which crack initiation has been observed. The computed time to initiation is found to occur at point C11_m80i, result which is in accordance with experimental observations. Both the time and the location of the crack initiated are gained by the present damage analysis.

TAB. 3: *Computed time of crack initiation*

Distance from the axis of cold water pipe	Points	$\frac{t_R \text{ computed}}{t^{\text{exp}}_{\text{C11m80i}} \text{at inspection } n}$	$\frac{t_R \text{ computed}}{t^{\text{exp}}_{\text{C11m80i}} \text{at inspection } n+1}$
194 mm	C11_m50i	7.7	5.1
	C11_m60i	2.2	1.5
	C11_m70i	2.9	1.9
	C11_m80i	$\boxed{1.2}$	$\boxed{0.8}$
	C11_m90i	1.7	1.1
	C11_p90i	2.41	1.6
344 mm	C14_m50i	> 16.9	> 11.2
	C14_m60i	> 16.9	> 11.2
	C14_m70i	> 16.9	> 11.2
494 mm	C21_m60i	> 16.9	> 11.2
644 mm	C24_m70i	> 16.9	> 11.2

Still by use of DAMAGE_2005, one can also plot the damage history over one cycle, i.e. over the 10 seconds of loading (Fig. 12). One notices that due to the consideration of an asymptotic fatigue limit, the damage mainly evolves

part by part. This expresses the fact that from the whole 10 seconds loading sequence, only some loads have a significant (damaging) effect on the material. This emphasizes once more the difficulty to define equivalent cycles, difficulty avoided in the present incremental analysis by computing the complete time increment by time increment material response.

FIG. 12: *Damage evolution over the 10s sequence (D vs normalized time $t/10s$)*

6.2 Application to INTHERPOL experiment

A second thermal fatigue test called INTHERPOL has also been developed in the framework of THERFAT European project in order to obtain experimental data still on crack initiation and propagation under high cycle thermal fatigue loadings (Curtit, 2004). The INTHERPOL01 testing structure is a 304L stainless steel pipe comprising a taper and an un-flushed circumferential welded joint (Fig. 13). It is subjected to cyclic thermal loadings with known amplitude and frequency. The pipe outside diameter is 406 mm, its thickness 10 mm and its height 300 mm. The welding is located at 200 mm from the bottom of the specimen. Before beginning thermal cycling, the structure is heated up to a homogeneous temperature of 230°C. Thermal cycling is carried out on a 70 mm broad sector of the internal surface of the specimen.

FIG. 13: *INTHERPOL01 pipe geometry (length in mm)*

The thermal loading device is described in figure 14. A cold thermal shock is generated by the pulverization of a cold water spray while the more gradual temperature increase is obtained by subjecting the cooled surface to an intense infra-red radiation and by an alternate mock up rotation. The 5 seconds thermal cycle breaks up into 3.5 seconds of heating, 0.15 second of transition, 1.2 seconds of cooling and 0.15 second of transition (Fig. 15). The thermal amplitude is 120°C (in fact between 110 and 130°C depending on the considered point).

FIG. 14: *Description of the thermal loading service*

FIG. 15: *Load sequence and thermal evolution at point A4*

During the fatigue test, the temperature is measured in different points on the internal surface (corresponding to thermocouples Ai of figure 16). The recording of the amplitudes of temperature is given in figure 17. as a ΔT versus normalized time $t/5s$.

FIG. 16: *Points Ai of thermocouples location*

FIG. 17: *Temperature recording over a cycle*

The thermal fatigue test is periodically stopped in order to detect the initiation (and propagation) of cracks by liquid penetrant inspections. During the whole test, approximately 265 000 cycles were carried out. The first crack was observed during the fourth liquid penetrant inspection after 124 263 cycles. At the end of the test, 18 cracking indications were observed (one in taper and 17 in current zone). The graph of figure 18 gives a summary of the test cracking history. We will notice during the first cycle of loading that the maximal damage appears at the point A4 though the amplitude ΔT is superior at the point A5 (C_5 in the figure). This can be explained by a higher thermal gradient during the cold thermal shock at the point A4 and hence a more important increase in stress. This is taken into account by the two scale model thanks to the damage evolution law governed by the accumulated plastic strain rate.

FIG. 18: *Evolution of the cracks lengths for the five cracks observed during inspection 5*

For each position of the thermocouples distributed on the median generatrix of sector test (on the inner surface), the results from a thermo-elastic computation are the temperature and strain histories during the 5s cycle (Curtit, 2004). An example of both the temperature and the stress fields obtained is given in figure 19. These datas are the inputs for DAMAGE_2005 post-processor which allows to determine the number of repetitions of the complex thermo-mechanical cycle necessary for the initiation of a crack. The set of parameters used are those for 304L steel. They are given in previous tables 1 and 2.

FIG. 19: *Temperature and stress fields on the internal surface of INTHERPOL01 cylinder from a Finite Element analysis*

The numbers of cycles and the times of crack initiation computed over the 10 Ai-points are presented in table 4. It is shown that initiation of the first crack occurs at the point A5 after 143000 cycles or 198 hours to be compared to the inspection number of cycles of 124000 or the corresponding time of 172 hours. These results are in accordance with the experimental observations from both the location and the order of magnitude points of view.

One can also plot the computed damage evolution during the first cycle of loading (figure 20) for the different points Ai. The damage does not evolve much during the heating stage. Most of the damage is due to the cold shock (around 0.9 of normalized time or t=4.5 seconds of real time). And D is of course larger for point A5 at which the crack initiates.

FIG. 20: *Damage evolution over the 5s sequence (D vs normalized time $t/5s$)*

TAB. 4: *Numbers of cycles and times to crack initiation*

Points	N_R (cycles)	Time (hours)
A1	$> 1.41\,10^7$	> 19600
A2	$> 1.41\,10^7$	> 19600
A3	$1.14\,10^6$	1579
A4	$3.35\,10^5$	465
A5	$1.43\,10^5$	198
A6	$3.67\,10^5$	509
A7	$5.26\,10^5$	731
A8	$3.92\,10^5$	545
A9	$1.81\,10^6$	2514
A10	$> 1.41\,10^7$	> 19600

7 Conclusion

The two scale damage model is a constitutive model for damage and High Cycle Fatigue. It allows to compute the mesocrack initiation conditions in complex mechanical, thermal and thermo-mechanical fatigue as it has been illustrated. The model being written in an incremental or rate form (in opposition to a stress or strain amplitude forms), it naturally allows to deal with random fatigue and there is no need of arbitrary equivalent cycles. The model is implemented in a post-processor form, post-processor DAMAGE_2005 of Finite Element 3D computations. A robust numerical scheme allows for the computation of millions of cycles in few minutes on a PC.

One has performed successfully damage post-processing of thermo-hydraulic computations (giving the temperature fields) followed by thermo-elastic computations (giving the complex strains and stresses history). The structures studied were INTHERPOL01 mock up and FATHER real size testing structure representative of pressure vessels subjected to complex temperature variation due to inside vessel chaotic mixture of hot and cold fluids. The times to crack initiation are obtained from the proposed damage analysis and satisfactory compared with the experimental results.

Further modeling is the extension to stochastic aspects. From the loading point of view, DAMAGE_2005 allows for random fatigue calculations as it is built on a rate form damage model. From the material point of view, effects of defects heterogeneity can in a first approach be phenomenogically handled by making the asymptotic fatigue limit probabilistic (Lemaitre and Desmorat, 2005; Doudard et al., 2005).

Références

Aas-Jackobsen, K. and Lenshow, R. (1973). Behavior of reinforced columns subjected to fatigue loading. *ACI Journal*, 70:199–206.

Angles, J., Taheri, S., and Papaconstantinou, T. (2005). High cycle fatigue under multiaxial loading damage, accumulation models applied to an industrial structure. In *18th International Conference on Structural Mechanics in Reactor Technology (SMiRT 18), Beijing, China, August 7-12*.

Beaud, F., Balançon, T., Stephan, J., Dumez, C., Amzallag, C., Le-Duff, J., Volte, O., and Robert, N. (2006). Identification des zones de mélange sensibles à la fatigue thermique. In *Prix SFEN (French Nuclear Society), common paper EDF and AREVA NP*.

Chaboche, J. and Lesne, P. (1988). A non-linear continuous fatigue damage model. *Fatigue Fract. Engng Mater. Struc.*, 11:1–17.

Charkaluk, E. and Constantinescu, A. (2000). An energetic approach in thermomechanical fatigue for silicon molybdenum cast iron. *Materials at High Temperatures (UK)*, 17:373–380.

Crossland, B. (1956). Effect of large hydrostatic pressures on the torsional fatigue strength of an alloy steel. *Proc. of the Inter. Conf. on fatigue metals Inst. Mech. Engr.*, pages 138–149.

Curtit, F. (2004). Intherpol thermal fatigue tests. In *Third International Conference on fatigue of Reactors Components – October 3-6, 2004 – Seville, Spain*.

Curtit, F. and Stephan, J.-M. (2005). Mechanical aspect concerning thermal fatigue initiation in the mixing zones piping. In *18th International Conference on Structural Mechanics in Reactor Technology (SMiRT 18), Beijing, China, August 7-12*.

Dang-Van, K. (1973). Sur la résistance à la fatigue des métaux. *Sciences et Techniques de l'Armement*, 3:647–722.

Dang-Van, K. and Papadopoulos, I. (1999). *High Cycle Metal Fatigue*. Springer, New York.

Desmorat, R. (2000). Modélisation et estimation rapide de la plasticité et de l'endommagement, habilitation à diriger des recherches. Technical report, Université Pierre et Marie Curie.

Desmorat, R. and Lemaitre, J. (2001). *Two scale damage model for quasi-brittle and fatigue damage, chapter Continuous Damage, section 6.15*, pages 525–535. Ed. J. Lemaitre, Academic Press.

Desmorat, R., Pauget, F., and Sermage, J.-P. (2006). Damage-2005: a post-processor for high cycle fatigue under complex thermomechanical loading. In *ASME Pressure Vessels and Piping Division Conference, Vancoucer, BC, Canada, 23-27 july*.

Doudard, C., Calloch, S., Cugy, P., Galtier, P., and Hild, F. (2005). A probabilistic two-scale model for high cycle fatigue life predictions. *Fatigue & Fracture of Engineering Materials & Structures*, 28:279–288.

Dupas, P. and Waeckel, F. (1997). Recueil bibliographique de caractéristiques thermo-mécanique pour l'acier de cuve, les revêtements inoxydable et les alliages 182 et 600. Technical Report HI-74/93/097, EDF-R&D.

Eshelby, J. D. (1957). The determination of the elastic field of an ellipsoidal inclusion, related problems. *Proc. Roy. Soc., London*, A241:376.

Faidy, C. and Le-Duff, J. (2006). Hich cycle thermal fatigue issues in pwr's lessons learned from field experience and consequences. In *International symposium on contribution of materials investigaion to improve the safety and performane of LWRs, International Conférence SFEN, Fontevraud, France, september 18-22.*

Fatemi, A. and Yang, L. (1998). Cumulative fatigue damage and life prediction theories: a survey of the state of the art for homogeneous materials. *International Journal of Fatigue*, 20:9–34.

Hua, C. and Socie, D. (1984). Fatigue damage in 1045 steel under constant amplitude biaxial loading. *Fatigue Eng. Mat. Struct.*, 7:165–179.

Kröner, E. (1961). On the plastic deformation of polycrystals. *Acta Metall.*, 9:155–161.

Kujawski, D. and Ellying, F. A. (1984). A cumulative damage theory of fatigue crack initiation and propagation. *International Journal of Fatigue*, 6:83–88.

Leiholz, H. H. E. (1986). On the modified s-n curve for metal fatigue prediction and its experimental verification. *Engineering Fracture Mechanics*, 23:495–505.

Leis, B. N. (1988). A nonlinear history-dependent damage model for low cycle fatigue. In H. D. Salomon, G.R. Halford, L. K. and Leis, B., editors, *Low Cycle Fatigue, ASTM STP 942, American Society for Testing Materials, Philadelphia, P.A., USA*, pages 143–159.

Leis, B. N. (1997). An energy-based fatigue and creep-fatigue damage parameter. *Journal of of Pressure Vessels and Technology, ASME Transactions*, 99:524–533.

Lemaitre, J. (1992). *A Course on Damage Mechanics*. Springer Verlag.

Lemaitre, J. and Chaboche, J. L. (1985). *Mécanique des matériaux solides*. Dunod (english translation 1990 'Mechanics of Solid Materials' Cambridge University Press).

Lemaitre, J. and Desmorat, R. (2001). *Isotropic and anisotropic damage law evolution*, chapter Handbook of Materials Behavior Models, Continuous Damage, section 6.14, pages 513–524. Ed. J. Lemaitre, Academic Press.

Lemaitre, J. and Desmorat, R. (2005). *Engineering Damage Mechanics : Ductile, Creep, Fatigue and Brittle Failures*. Springer.

Lemaitre, J. and Doghri, I. (1994). Damage 90 : a post processor for crack initiation. *Comput. Methods Appl. Engng.*, 115:197–232.

Lemaitre, J. and Plumtree, A. (1984). Application of damage concepts to predict creep-fatigue failures. *J. Eng. Mat. Technol.*, 101:284–292.

Lemaitre, J., Sermage, J. P., and Desmorat, R. (1999). A two scale damage concept applied to fatigue. *International Journal of Fracture*, 97:67–81.

Manson, S. S. and Halford, G. R. (1986). Re-examination of cumulative fatigue damage analysis – an engineering perspective. *Engineering Fracture Mechanics*, 25:539–571.

Manson, S. S. and Hirschberg, M. (1964). *Fatigue: An Interdisciplinary Approach*. Syracuse University Press, Syracuse, N.Y.

Miner, M. A. (1945). Cumulative damage in fatigue. *J. Appl. Mech.*, 67:A159–A164.

Paas, M. (1990). *Continuum damage mechanics with an application to fatigue*. PhD thesis, Eindhoven University of Technology, The Netherlands.

Pasutto, T., Péniguel, C., and Sakiz, M. (2005). Chained computation using an unsteady 3d approach for the determination thermal fatigue in a t-junction of a pwr nuclear plant. In *ICAPP – Seoul*.

Robert, N., Economou, J., Cornuel, F., Volte, O., and Stephan, J. (2006). Investigation of mixing zones subject to thermal fatigue. In *International symposium on contribution of materials investigaion to improve the safety and performane of LWRs SFEN, Fontevraud, France, 18-22 september*.

Sauzay, M. (2000). *Effet de surface libre en fatigue policyclique*. PhD thesis, Université Paris 6.

Seyedi, M., Desmorat, R., and Sermage, J.-P. (2004). A two scale model for thermo-mechanical high cycle fatigue failure. In *European Conference on Fracture ECF 15, Advanced Fracture Mechanics for Life and Safety, Stockholm, Sweden*.

Shigley, J. and Mischke, C. (1989). *Mechanical engineering design, 5th ed.* McGraw-Hill.

Sines, G. (1959). *Behavior of metals under complex static and alternating stresses*, pages 145–169. G. Sines and J. L. Waisman. McGraw Hill New York.

Taheri, S. (2004). High cycle thermal fatigue on a mixing zone of auxiliary cooling system. In *ASME-PVP conference, San Diego*.

Taheri, S. (2007). Some advances on understanding of high cycle thermal fatigue crazing. *Journal of Pressure Vessel Technology*, in press.

Taheri, S. and Doquet, V. (2001). Evaluation of non conservatism of combined rainflow counting and miner's rule for damage cumulation in strain controlled fatigue. In *16th International Conference on Structural Mechanics in Reactor Technology (SMiRT 16), Whashington D.C.*

Zuchowski, R. (1989). Specific strain work as both failure criterion and material damage measure. *Res. Mechanica*, 27:309–322.

List of Figures

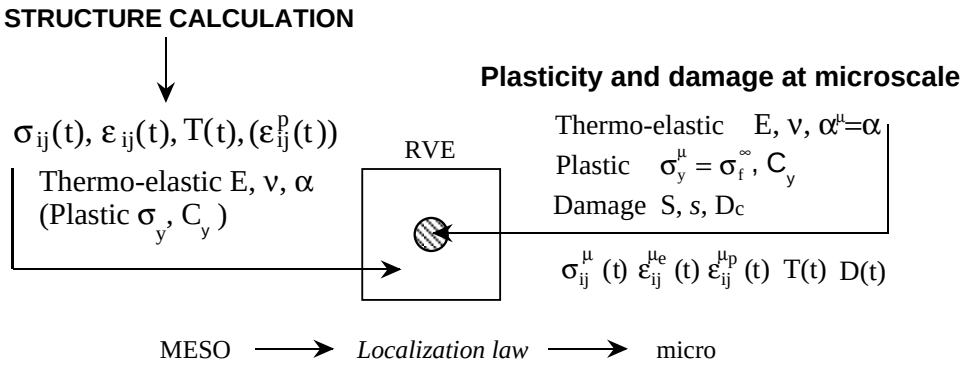

Figure 1: Micro-element imbedded in a thermo-elastic Representative Volume Element

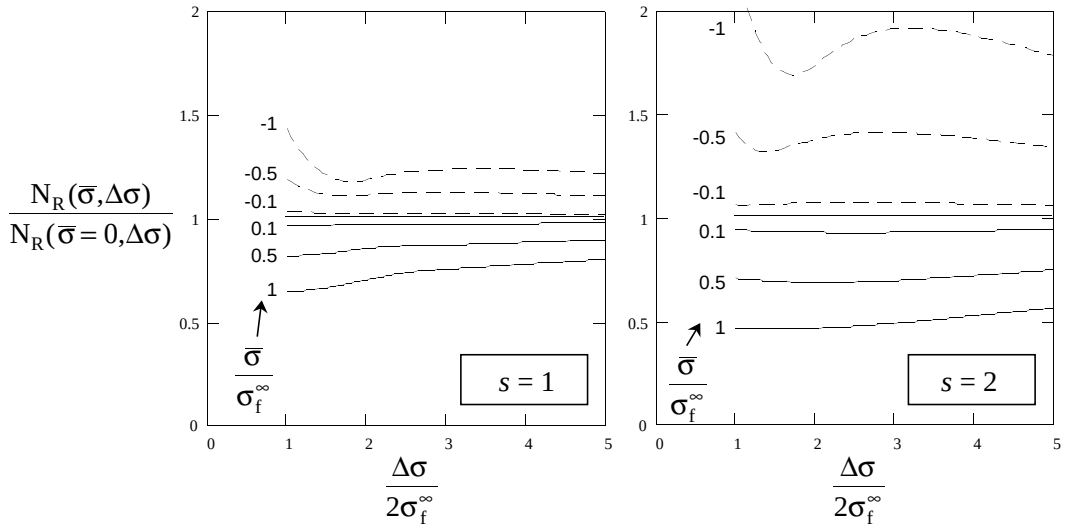

Figure 2: Mean stress effect – Curves plotted at constant ratio $\overline{\sigma}/\sigma_f^\infty$ for two values of the damage exponent s

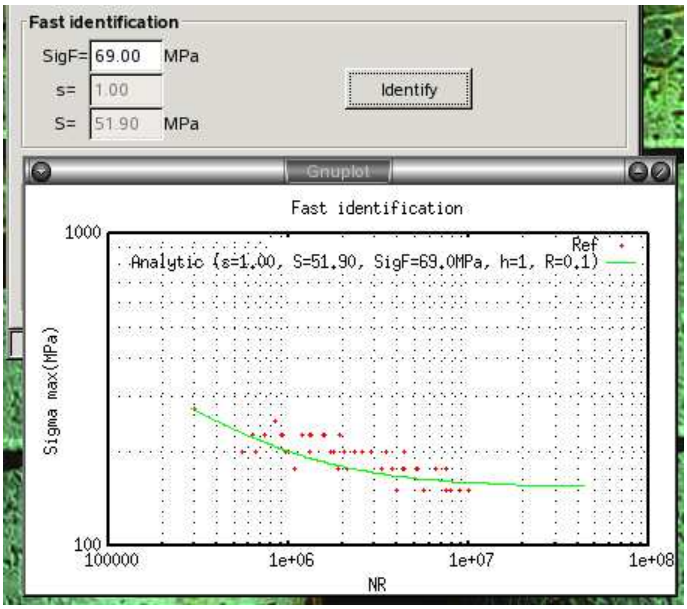

Figure 3: Fast identification procedure from approximate formula (**??**) with $h = 1$

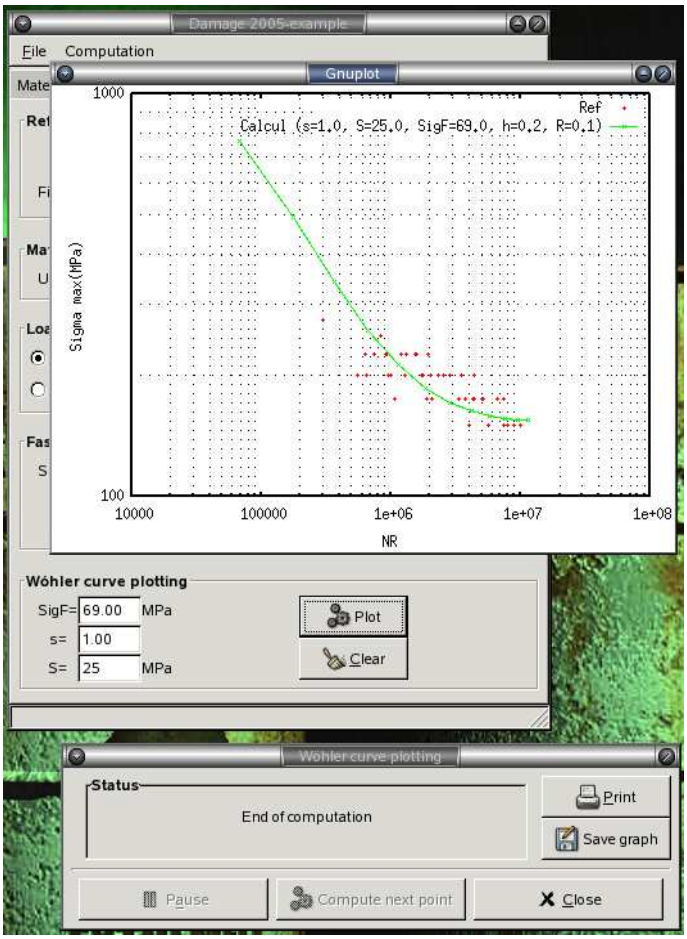

Figure 4: Final identification of S with $h = 0.2$

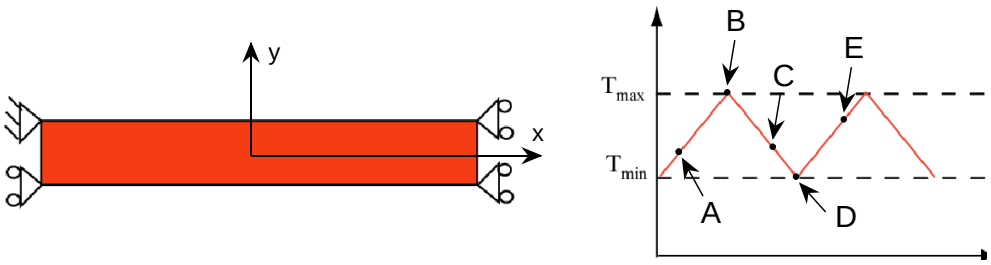

Figure 5: Thermal fatigue of a beam

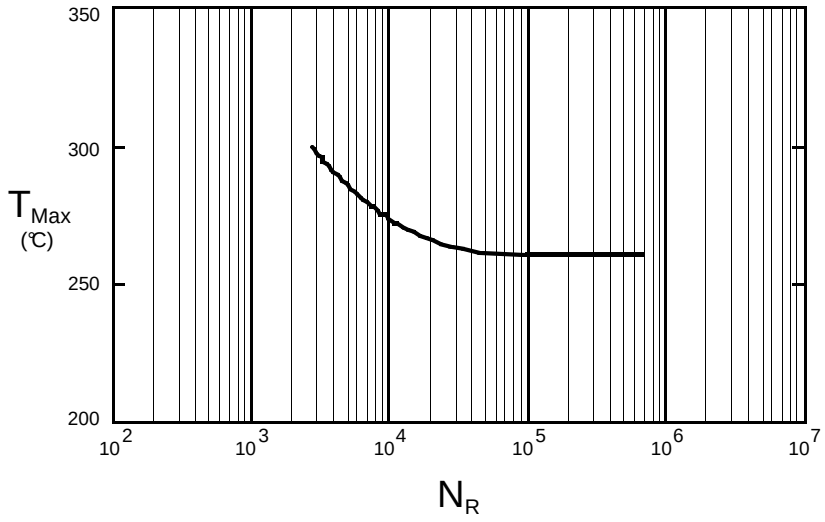

Figure 6: Computed thermal fatigue curve

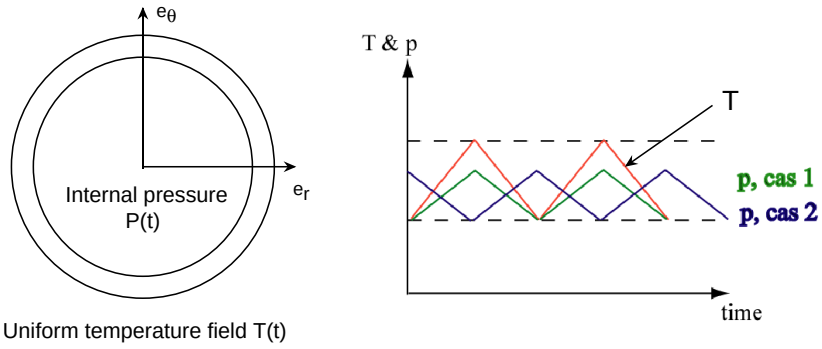

Figure 7: Thermomechanical fatigue of a pipe with internal pressure

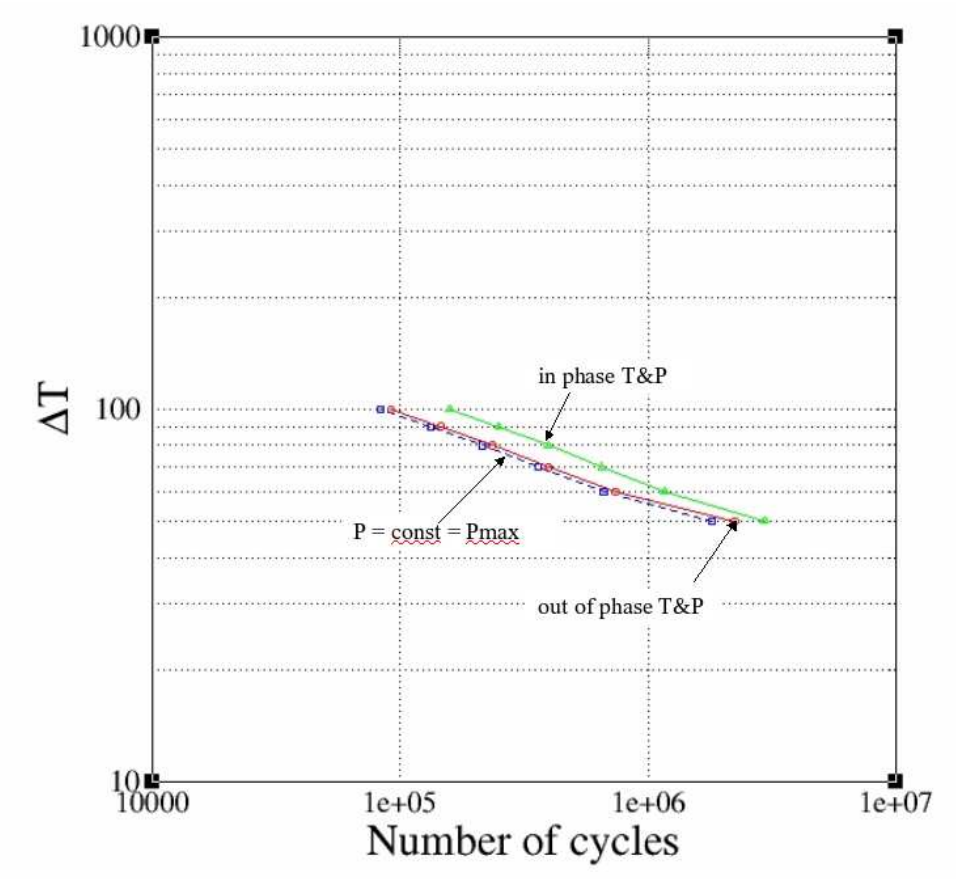

Figure 8: Thermomechanical fatigue – in phase (case 1), out of phase (case 2) loadings and loadings at constant pressure

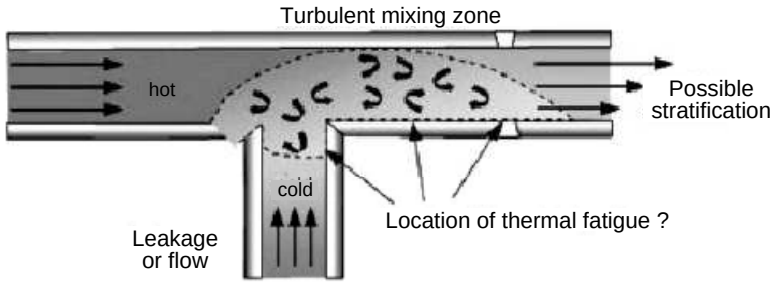

Figure 9: Turbulent temperature mixing in T-configuration

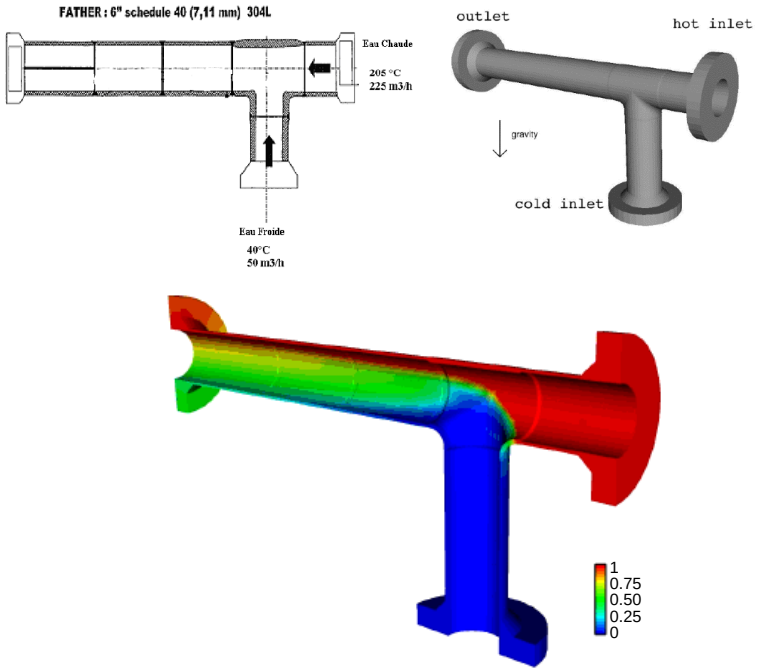

Figure 10: FATHER testing structure and computed instantaneous non dimensional temperature field(time=10s)

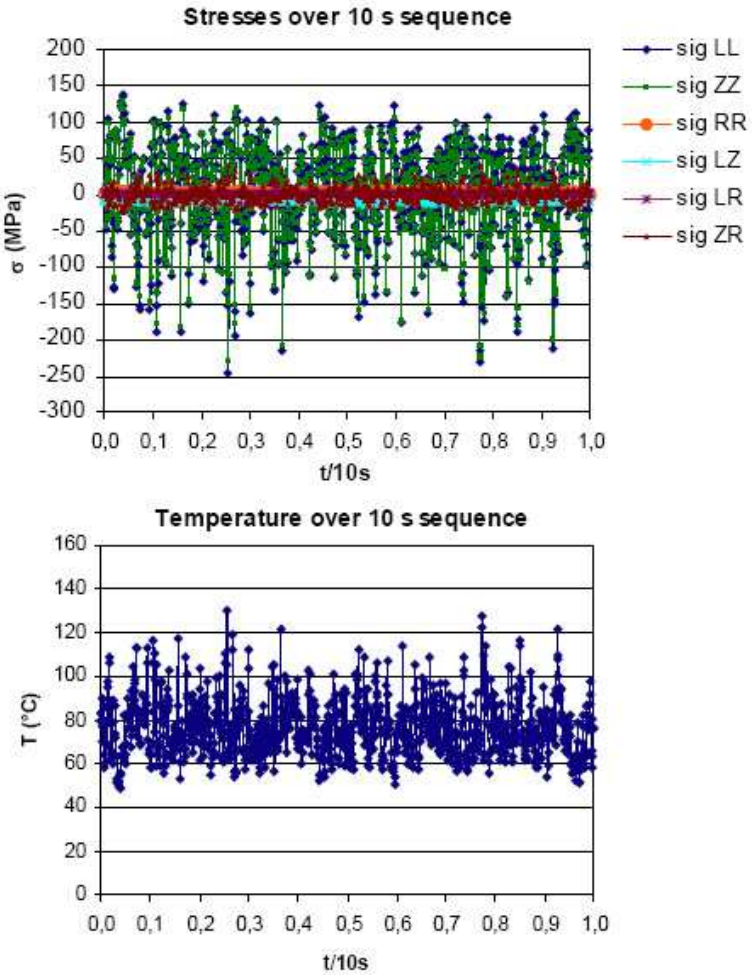

Figure 11: Loading sequence made of 1000 instants

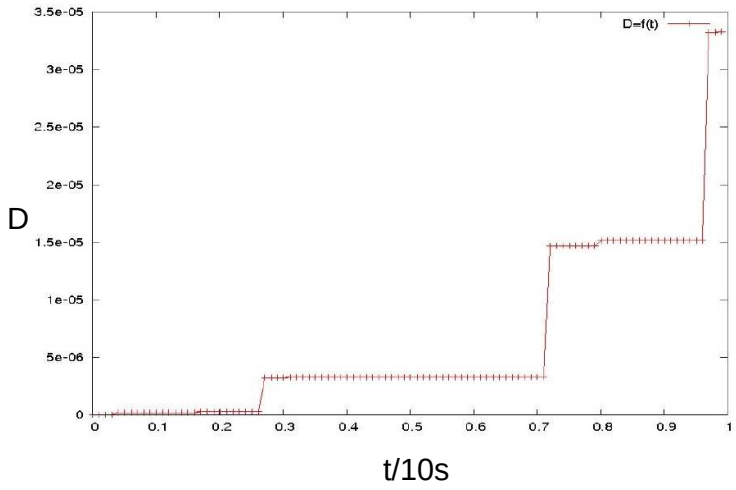

Figure 12: Damage evolution over the 10s sequence (D vs normalized time $t/10s$)

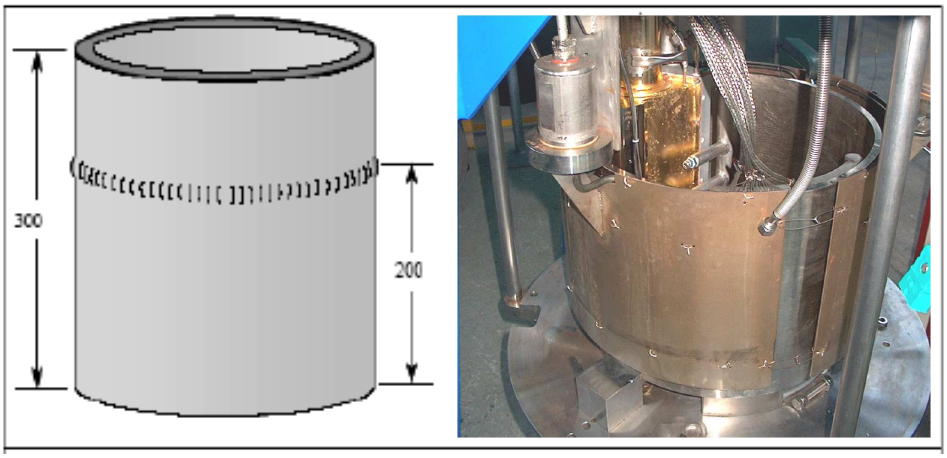

Figure 13: INTHERPOL01 pipe geometry (length in mm)

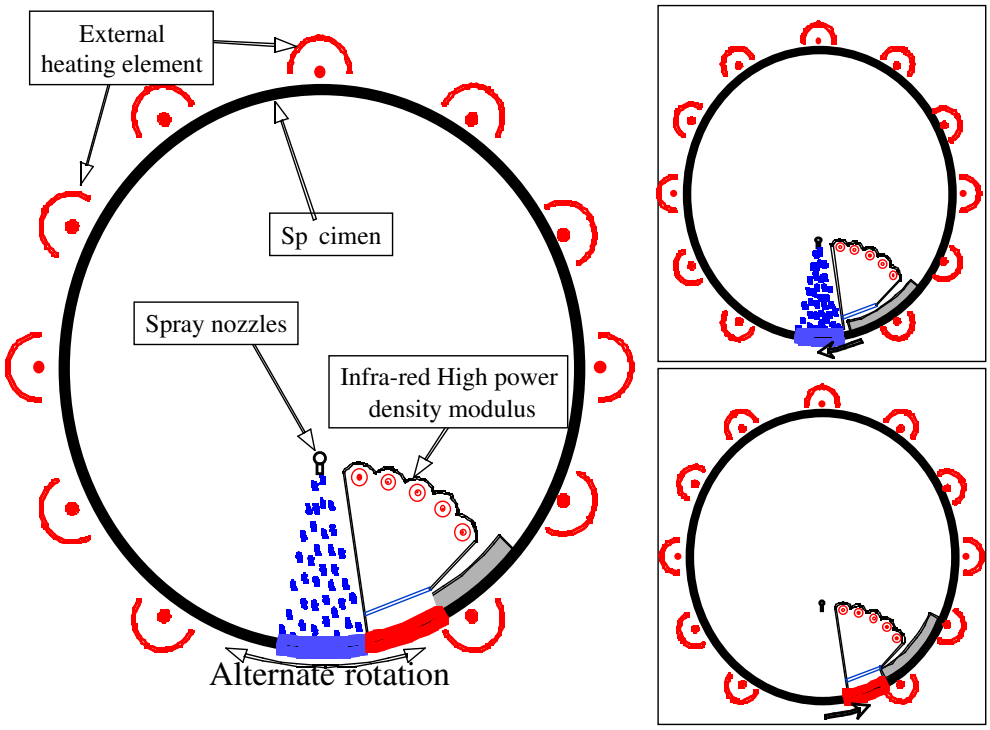

Figure 14: Description of the thermal loading service

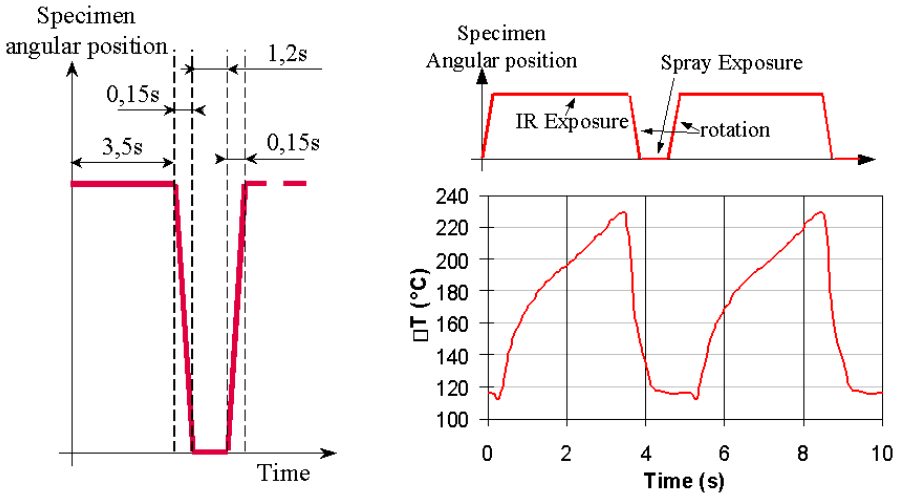

Figure 15: Load sequence and thermal evolution at point A4

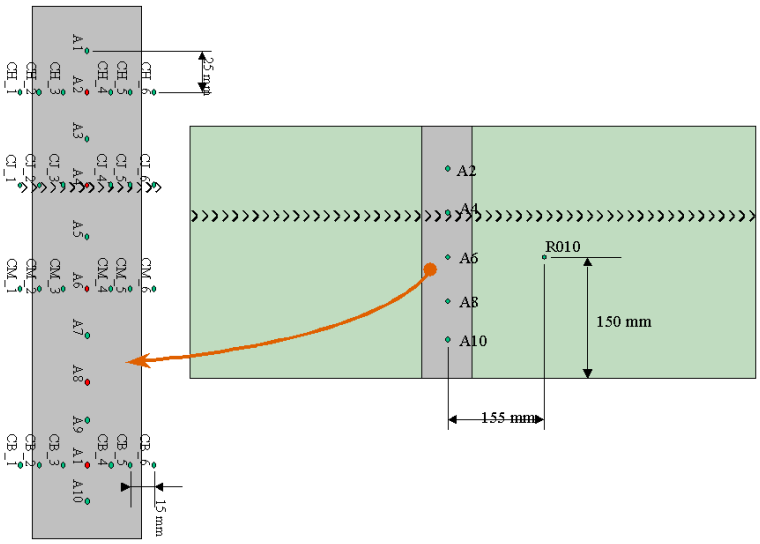

Figure 16: Points Ai of thermocouples location

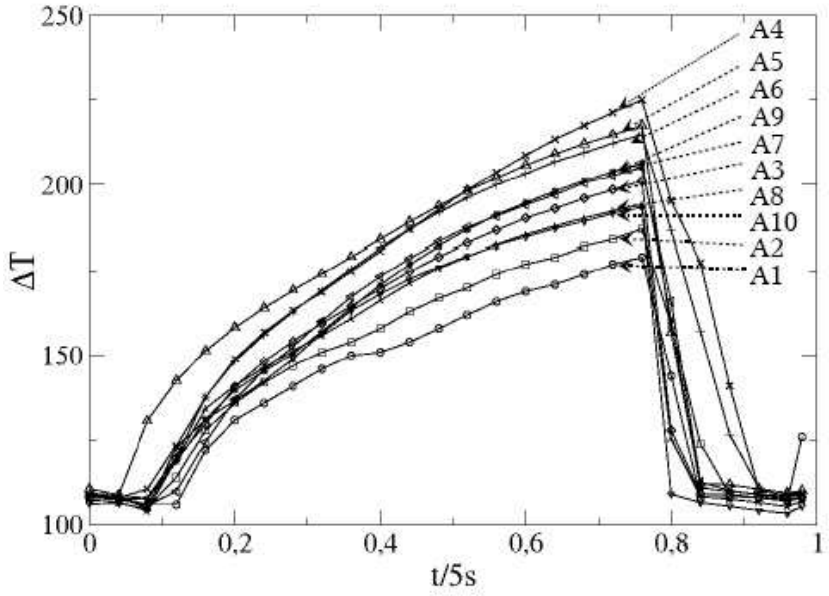

Figure 17: Temperature recording over a cycle

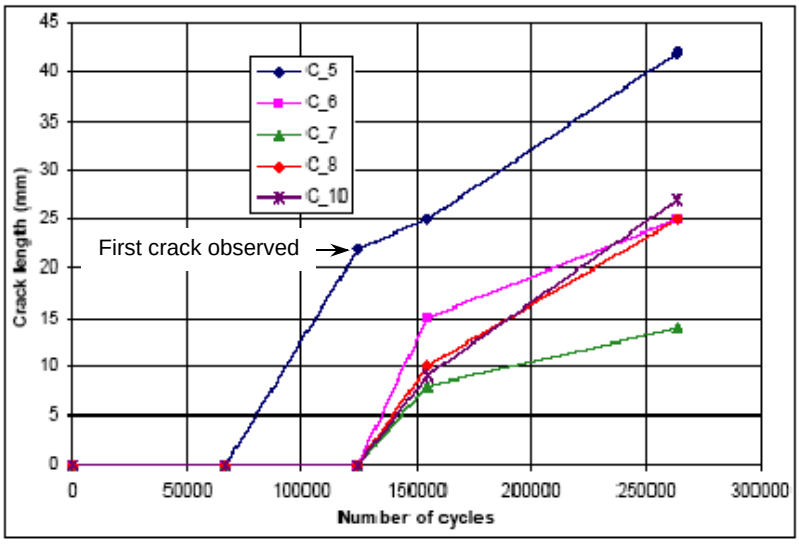

Figure 18: Evolution of the cracks lengths for the five cracks observed during inspection 5

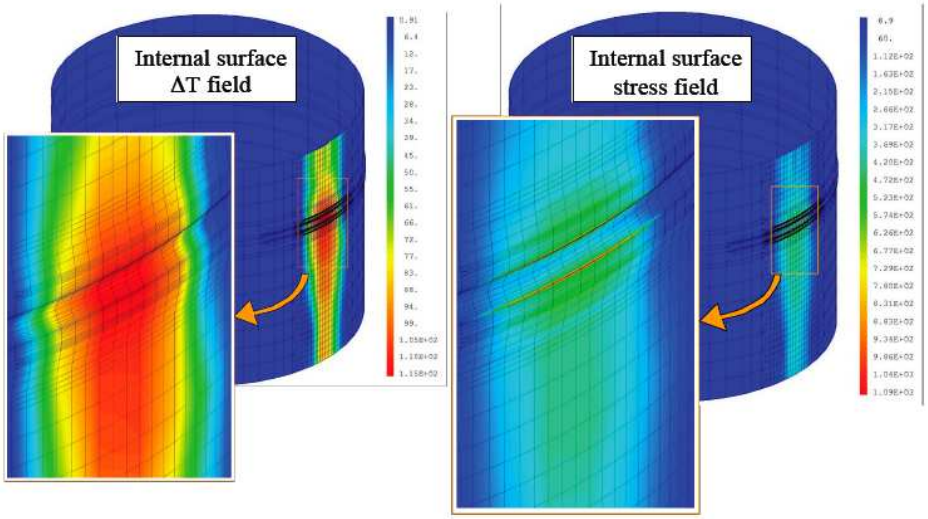

Figure 19: Temperature and stress fields on the internal surface of INTHER-POL01 cylinder from a Finite Element analysis

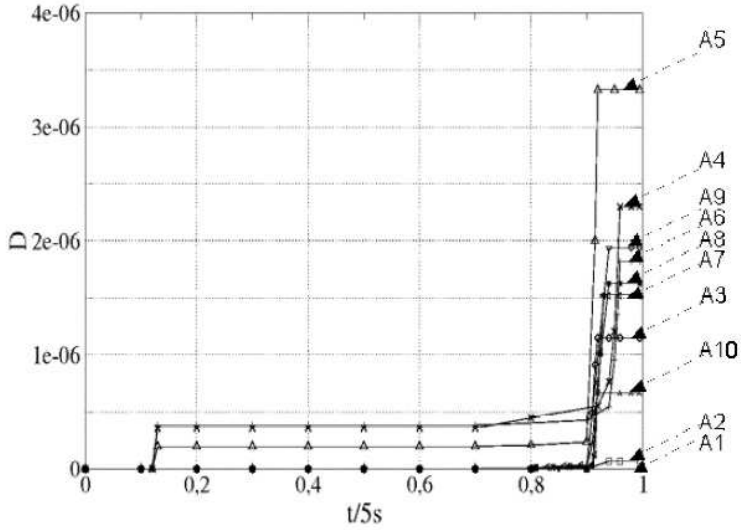

Figure 20: Damage evolution over the 5s sequence (D vs normalized time $t/5s$)